



Cadmium Oxide-Zinc Oxide Nanocomposites Synthesized Using Waste Eggshell Membrane and Its In-Vitro Assessments of the Antimicrobial Activities and Minimum Inhibitory Concentration

Prashanna Suvaitha Sundara Selvam¹ · Gandhi Shree Chinnadurai² · Dhinakaran Ganesan¹ · Palani Perumal² · Venkatachalam Kandan¹

Received: 7 July 2020 / Accepted: 25 July 2020 / Published online: 4 August 2020
© Springer Science+Business Media, LLC, part of Springer Nature 2020

Abstract

The following study was performed chiefly to analyze the antimicrobial activity of CdO/ZnO-ESM nanocomposites. A unique method was used for the synthesis of CdO/ZnO-ESM nanocomposites using an eggshell membrane as a bio-template which acts as both reducing and stabilizing agents; whereas cadmium nitrate and zinc nitrate were employed as metal precursors. The prepared samples were characterized by the following techniques such as TGA, PXRD, DRS–UV–Visible reflectance, FT-IR, HR-SEM, EDAX, Zeta potential, and Photoluminescence analysis. The prepared samples were subsequently tested for antimicrobial activity against Gram-positive bacteria (*Staphylococcus aureus* and *Bacillus* sp.) and Gram-negative bacteria (*Escherichia coli*, *Klebsiella pneumonia*, *Pseudomonas aeruginosa*, *Salmonella enterica*, and *Vibrio* sp.) using agar well diffusion method. The minimum inhibitory concentration was determined by the broth microdilution method. The maximum inhibition zone of 24 mm, was observed in *Salmonella enterica* at a concentration (30 µg/mL) of CdO/ZnO-ESM nanocomposites, while the highest MIC value was observed in *Bacillus* sp. at a concentration (1.95 µg/mL) of these nanocomposites. The result of this study showed that CdO/ZnO-ESM nanocomposites have an exceptional antimicrobial activity against both Gram-positive and Gram-negative bacteria.

Keywords Cadmium oxide · Zinc oxide · Eggshell membrane · Nanocomposites · Antimicrobial activity · Minimum inhibitory concentration

1 Introduction

Metal oxide nanoparticles have fascinated scientists owing to their noticeable characteristics like chemical stability and biocompatibility. These nanoparticles are also popular for the roles they offer in fields of applications in drug delivery, targeted therapeutics, enzymatic or metabolic degradation, detection of pathogenic species, tissue repair, hyperthermia and antigen diagnosis. Infectious diseases pose a potential threat to the mankind, particularly with the development

of antibiotic-resistant bacterial strains. Both gram-positive and gram-negative bacteria are a significant health concern. For several years, antibiotics are being used to combat community and hospital-related infections [1]. As we all know, antibiotics have the greatest therapeutic effect on bacterial infections. The major issue emerges from inadequate use, overuse and misuse of antibiotics for prophylactic and therapeutic purposes without sufficient medical guidance, thus due to bacterial resistance to antibiotics [2].

To overcome this issues, recent advancements in the fields of nanoscience and nanotechnology host new channels for us to benefit from. One of the applications to be explored to prepare oxides of certain metal (nanomaterials) of a specific sizes and shapes tend to show antimicrobial properties against bacteria, viruses and other pathogenic microorganisms. In addition, the properties of nanomaterials viz.: less than 100 nm in diameter with large surface to volume ratio, structure, solubility; makes them promising when it comes to efficiency in terms of usage or application

✉ Venkatachalam Kandan
venkatachalam@unom.ac.in

¹ Department of Analytical Chemistry, University of Madras, Guindy Campus, Chennai, Tamil Nadu 600025, India

² Centre for Advanced Studies in Botany, University of Madras, Guindy Campus, Chennai, Tamil Nadu 600025, India

in real-life predominantly in the medical industry due to their anti-microbial nature and the fact that they tend to penetrate easily into the bacterial cells [3]. The key mechanism of these nanoparticles influence on these pathogenic cells is thought to be DNA and protein damage as well as the destruction of the cell wall [4]. As a result, nanomaterials may serve as an alternative to antibiotics to combat bacterial infections. Antimicrobial agents of nanomaterials are generally classified as organic or inorganic agents. Inorganic nanomaterials, such as metal oxide nanoparticles, have become promising candidates because they are more stable, less toxic and more selective than organic nanomaterials. A variety of metal oxide nanomaterials such as ZnO, Fe₂O₃, TiO₂, CaO, MgO and CuO have been used as effective bacterial agents [3]. Latterly, binary metal oxide nanomaterials have been extensively utilized as an effective biocide agent for a wide variety of applications, such as thin-layer, anti-fouling thick coatings, fabrics, filter membranes, dental and biomedical applications [5].

Both ZnO and CdO are n-type semiconductors, while ZnO has a direct bandgap of 3.2 eV with a binding energy of value 60 mV [6], the direct bandgap of CdO remains to be 2.5 eV with an indirect bandgap of 1.98 eV. This difference in both direct and indirect is due to intrinsic cadmium and oxygen vacancy [7, 8]. Due to these extraordinary physical properties displayed by ZnO and CdO nanomaterials, they are used extensively in the manufacturing of optoelectronic devices, viz ultraviolet sensors, photocatalysts, photovoltaic cells, data storage and also in the field of biological applications owing to its low-cost, large surface area and catalytic activity [6, 9].

CdO and ZnO nanomaterials have the lowest toxicity compared to other semiconductor nanoparticles, amongst which HgO and PbO stand first in toxicity. These days, the majority of multivitamin tablets and dietary supplements consist of cadmium. In addition, CdO is present in a number of cosmetics and anti-tan creams. As a result, CdO can be found to be chemically well-matched with the body moiety. The thought-provoking fact about the anticancer features of CdO and ZnO nanostructures is that they are not harmful to human and mammalian cells [4]. Among the various metal oxides nanomaterials, CdO and ZnO have unique properties either individually or in composition. One of the most important combinations of CdO and ZnO nanocomposites has received more interest in the field of biological activity [10].

The literature survey showed that there are many methods available for the synthesis of CdO/ZnO nanocomposites as shown in Table 1. The above-mentioned approaches, either a physical or a chemical approach require high pressure/use of harsh chemicals and volatile solvents with a low yield, hazardous by-products, and remain to be time-consuming. To tackle these consequences, there persists a requisite to

synthesize nanomaterials with non-toxic solvents or reagents which make them cost-effective and perhaps less time-consuming. This is why the biosynthetic approach fulfils these conditions. The use of biological sources is present in nature such as plant products (flowers, roots, leaves, fruits, and barks), algae, fungi, bacteria, viruses, and biodegradable waste materials. Nowadays, the bio-waste mediated synthesis of nanomaterials is of significant interest as this method is very quick, scalable, and cost-effective. Some of the bio-waste materials used for nanoparticle synthesis are Citrus grandis, Citrus sinensis, Musa paradisiacal, and Eggshell membrane [29].

The concern is to make it low-cost and non-hazardous; the most available bio-waste is the eggshells. The eggshell membrane (ESM) serves as a bio-template, reducing, and stabilizing agents while containing various collagen proteins such as amino acid types—I, V, and X along with glycine, alanine, and uronic acid. ESM also contains functional groups of amino, carboxyl, carbonyl, and aldehydes [30]. There exists few literatures for the synthesis of metal, its oxides and nanocomposites using ESM which include SnO₂ [30], β-NiMoO₄ [31], gold nanoparticles [32, 33], SnO₂ [34], Co₃O₄ [35], copper-containing bioactive glass/ESM nanocomposite [36], Ag nanoparticles [37], CeO₂ [38], MnO₂ [39], TiO₂ [40], ZnO [41] and α-Fe₂O₃ [42]. The synthesis of CdO/ZnO-ESM nanocomposites using ESM as a bio-template, reducing and stabilizing agent has not been reported till date. Their application in the antimicrobial activity of Gram-positive bacteria (*Staphylococcus aureus* and *Bacillus* sp.) and Gram-negative bacteria (*Escherichia coli*, *Klebsiella pneumonia*, *Pseudomonas aeruginosa*, *Salmonella enterica*, and *Vibrio* sp.) were well studied and the results are discussed in comprehension below.

2 Methodology

2.1 Materials and Reagents

The Eggshells were collected from Anna University Canteen, Guindy campus, Chennai. Cadmium nitrate tetrahydrate (99%) and zinc nitrate hexahydrate (96%) have been purchased from Nice Chemicals (P) Ltd. (Kerala). Concentrated acid (HCl) was obtained from Sigma-Aldrich and the double-distilled water used in the experiment.

2.2 Preparation of Dried ESM

The collected eggshells were thoroughly washed with double-distilled water and the membrane was separated from the eggshells. The ivory-white ESM is rinsed with double-distilled water to get rid of any albumin and is left to dry at room temperature for about 2–3 days. The dry ESM is

Table 1 Synthesis of CdO/ZnO nanocomposites by using various methods

Methods	Calcination temperature (°C)	Time (h)	Crystallite size (nm)	Application	Refs.
Micro-wave assisted method	500	4	27.26	Antibacterial activity	[11]
Sol-gel method	600	8	45–65	–	[12]
Co-precipitation method	450	2	7.50	Photocatalytic degradation	[13]
Seaweed assisted-green approach	120	4	33.20	Photocatalytic degradation	[14]
Micro emulsion method	200, 400 and 600	–	–	Adsorption of dye removal	[6]
Thermal treatment method	600	90 min	14 to 32	Antibacterial activity	[10]
Wet-chemical method	450	4	155.2	Photocatalytic degradation	[15]
Ultrasound-assisted co-precipitation method	550	4	30–34	Photocatalytic degradation	[16]
Hydrothermal method	500	3	23	Photocatalytic degradation	[17]
Sol-gel method	70	–	140	–	[18]
Magnetron sputtering method	800	7	–	Antimicrobial	[5]
Electrodeposition method	600	6	22–25	–	[19]
Precipitation accompanied by hydrothermal method	500	4	57	Antibacterial	[20]
Wet chemical method	500	3	43	Photocatalytic activity	[21]
Homogeneous chemical co-precipitation method	450	4	28.85 and 57.70	Sono-catalytic and photocatalytic degradation	[22]
Sol-gel with co-precipitation method	550	4	41	Gas sensing	[23]
Vapor to the solid mechanism	350	3	25–54	Degradation and electrochemical detection	[24]
Honey-assisted combustion method	100–400	–	49	Antimicrobial	[25]
Hydrothermal method	60	–	34 ± 3	Photocatalytic activity	[26]
Hydrothermal method	150	5	–	Photovoltaic and sensing application	[27]
Screen printing technique on the glass substrate	–	–	25	Photovoltaic application	[28]
Eggshell membrane assisted CdO/ZnO-ESM nanocomposites	550	2	35	Antimicrobial activity	Present study

then soaked in a 10% HCl solution for about 20 min to eliminate the calcium carbonate present in the ESM. The soaked ESM is rinsed with double distilled water and dried yet another time as done earlier. The dry ESM is utilized for the synthesis.

2.3 Preparation of CdO/ZnO-ESM Nanocomposites and Pure Samples of CdO-ESM and ZnO-ESM Nanopowders

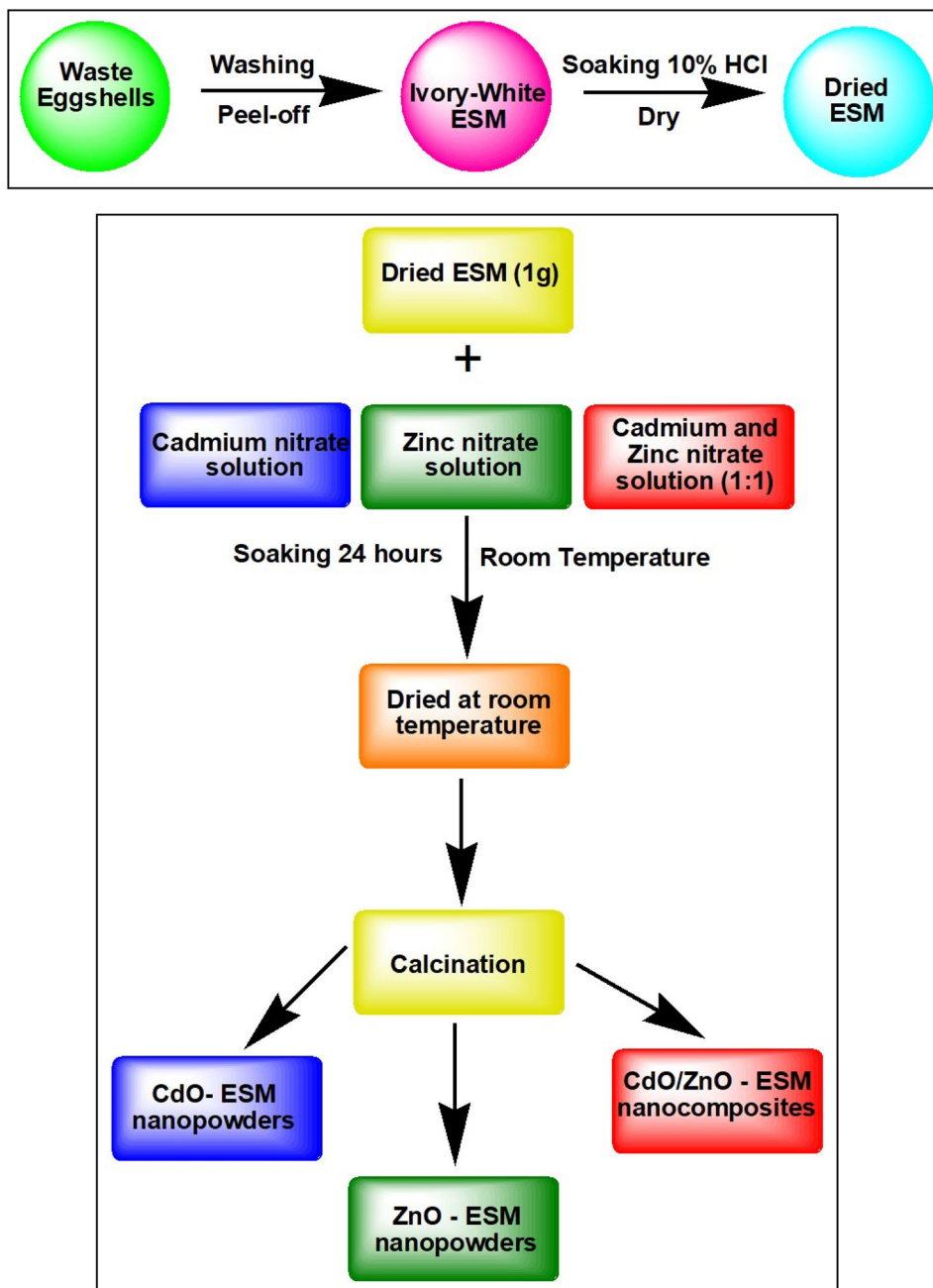
CdO/ZnO-ESM nanocomposites are synthesized as mentioned earlier by the procedure discussed in [43]. Usually, 1 g of dried ESM is soaked in 50 mL of 0.2 M/L cadmium nitrate and zinc nitrate solution ($V_{\text{Cd}}:V_{\text{Zn}} = 1:1$). After soaking for about 24 h, the color of ESM changes from white to pale yellow, indicating the existence of precursors of cadmium and zinc. The ESM is dried at room temperature and

then calcined at about 550 °C for 2 h. Pale brown colored nanocomposites were obtained. The sample is now labeled as CdO/ZnO-ESM nanocomposites. A similar technique for the preparation of CdO and ZnO nanopowders, and thus the samples were labeled as CdO-ESM nanopowders and ZnO-ESM nanopowders respectively. The Scheme of the preparation methods of CdO-ESM nanopowders, ZnO-ESM nanopowders, and CdO/ZnO-ESM nanocomposites as shown in Fig. 1.

2.4 Determination of Antimicrobial Activity by Agar Well Diffusion Method

Antimicrobial activity of CdO-ESM nanopowders, ZnO-ESM nanopowders, and CdO/ZnO-ESM nanocomposites were tested against both Gram-positive bacteria (*Staphylococcus aureus* and *Bacillus* sp.) and Gram-negative bacteria

Fig. 1 The Scheme of the preparation methods of CdO-ESM nanopowders, ZnO-ESM nanopowders and CdO/ZnO-ESM nanocomposites using Eggshell membrane as a bio-template reducing and stabilizing agents



(*Escherichia coli*, *Klebsiella pneumonia*, *Pseudomonas aeruginosa*, *Salmonella enterica*, and *Vibrio* sp.) is examined with the aid of agar-well diffusion process [44].

2.4.1 Preparation of Seed Inoculum

The test microorganisms were collected from the Microbiology Department, University of Madras, Taramani Campus, Chennai. In prior, the test microorganisms were placed under laboratory conditions in the Nutrient agar slants stored at 4 °C. A Muller Hinton broth is prepared

using commercially available Muller Hinton (33 g) in Hi Medium and is boiled with 1 L of double-distilled water. After it is completely soluble, the desired quantity of the medium is dispensed and sterilized at 15 lbs pressures and a temperature of 121 °C for about 15 min by autoclaving. Prior to the start of the experiment, bacterial cultures were inoculated into separate test tubes containing Muller Hinton broth and were placed in a rotary shaker incubator (180 rpm; 37 °C ± 2 °C) for about 24 h.

2.4.2 Agar Well Diffusion Method

A Muller Hinton agar is prepared by dissolving 33 g of Muller Hinton agar powder in 1 litre of double-distilled water. The mixture is then heated continuously with occasional stirring until the solute is completely dissolved. This mixture is sterilized with the aid of autoclaving at a pressure of 15 lbs and a temperature of 121 °C for about 15 min. After, it is left to cool down to room temperature, but not solidify. 20 mL of Muller Hinton agar is then transferred to each Petri-plate and is left on the sterile surfaces until the agar has solidified. The 24-h Muller Hinton broth culture of individual bacterial strains is seeded on a Petri-plate containing Muller Hinton agar medium using sterilized cotton swabs. For each Petri-plate, wells that are of 6 mm in diameter are made out of sterile steel cork borer. The prepared CdO/ZnO-ESM nanocomposites of concentration 1 mg/mL are dispersed into sodium acetate buffer solution which acts as a negative control (50 mM; pH 5.0) and are sonicated for about 30 min to obtain a uniform concentration. 30 µg/mL of CdO/ZnO-ESM nanocomposites was injected into each well. The plates had been incubated at a temperature of 37 °C ± 2 °C for about 24 h. Streptomycin of concentration 15 µg/mL has been used as a positive control. The zone of inhibition was measured after the first 24 h of incubation. A similar process had been performed for CdO-ESM nanopowders and ZnO-ESM nanopowders respectively.

2.5 Determination of Minimum Inhibitory Concentration (MIC) by Resazurin-Based Microdilution Assay

Resazurin-based microdilution assay is carried out to determine the minimal inhibition concentration of CdO-ESM nanopowders, ZnO-ESM nanopowders, and CdO/ZnO-ESM nanocomposites were tested against both Gram-positive bacteria (*Staphylococcus aureus* and *Bacillus* sp.) and Gram-negative bacteria (*Escherichia coli*, *Klebsiella pneumonia*, *Pseudomonas aeruginosa*, *Salmonella enterica*, and *Vibrio* sp.) [45]. Broth micro dilutions had been carried out under the Clinical and Laboratory Standards Institute (CLSI) protocol.

2.5.1 Preparation of the Bacterial Suspension

The test microorganisms have been sub-cultured on nutrient agar plates and incubated at about 37 °C ± 2 °C for about 24 h. After incubation, two to three discrete bacterial colonies are inoculated with identical morphology into 10 mL sterile Muller Hinton broth and incubated overnight at about 37 °C ± 2 °C. The resulting bacterial suspensions have been adjusted to 0.5 McFarland Standard with sterile Muller Hinton broth.

2.5.2 Preparation of Resazurin Dye Solution

Precisely weighed 334 mg of resazurin powder in 50 mL of sodium acetate buffer solution (50 mM; pH 5.0) and stirred to achieve homogeneity for 30 min. The process is performed under dark conditions and kept in an amber-colored standard flask to prevent light exposure.

2.5.3 Preparation of 96-Well Plates

96-well plates were made use of under sterilized conditions. A volume of 200 µL of CdO/ZnO-ESM nanocomposites (test sample) in 10% (v/v) of sterile water (mg/mL) was pipetted into the first row of the plate. 100 µL of Muller Hinton broth was then added to all other wells. Using the serial dilution method, the test samples were diluted in descending order and discarded in the last well of the test sample. 10 µL of resazurin dye solution had been added to each well. An additional 30 µL of Muller Hinton broth was added to each well to ensure that the final volume is the single strength of Muller Hinton broth. Finally, 10 µL of bacterial suspension had been added to each well. Each plate is loosely covered with a thin film to ensure that the bacteria are not dehydrated. Each plate has a set of controls, a column with a wide range of antibiotics (Streptomycin) as a positive control (medium + antibiotic + culture + resazurin dye solution); a column with all solutions except for the test compound as a negative control (medium + culture + resazurin dye). The plates were prepared in triplicate and placed in an incubator at a temperature of 37 °C ± 2 °C for about 18–24 h. The change in color was visually assessed. Any color changes from purple/blue to pink/red or colorless indicated the presence of viable cells. The lowest concentration before the color change was considered to be the minimum inhibitory concentration. The average of three values was calculated and the MIC value was determined. A similar study was carried out for CdO-ESM nanopowders and ZnO-ESM nanopowders.

2.6 Instrumentation Techniques

Thermal Analyzer-TGA (NETZSCH STA 2500) was recorded under the nitrogen atmosphere at a temperature range of 30–800 °C (heating rate of 10 °C step min⁻¹). The X-ray diffraction was carried out on 3000TT made in Germany, with an operating voltage of 40 keV, 30 Ma-Current rate, Target Cu. DRS UV–Visible Spectrophotometer-Perkin Elmer-650 DRS and Varian Cary Bio-100 were used to measure the DRS UV–Visible reflectance spectra. The FT-IR spectrum was recorded on SPECTROMETERS-THERMO iS50 within a range of 4000–400 cm⁻¹. A High-resolution scanning electron microscope (HR-SEM) with EDAX analysis was recorded on FEI-Quanta FEG 200F. The

zeta potential was computed using the Dynamic Light Scattering Instrument. Photoluminescence spectra were carried out with the aid of Spectro-fluorimeters-Horiba.

3 Results and Discussion

3.1 Thermogravimetric Analyses

The thermal stability of the dried ESM, CdO-ESM nanopowders, ZnO-ESM nanopowders, and CdO/ZnO-ESM nanocomposites was analyzed using NETZSCH STA 2500 TGA set up, operated at a temperature range of 30–800 °C.

3.1.1 Dried ESM

The TGA curve of dried ESM is shown in Fig. 2. The initial weight loss of 5% was noted below 100 °C, is due to the removal of moisture or physically adsorbed water molecules on the ESM surface. The major weight loss of 69% was recorded at a temperature range of 110–510 °C, is due to the decomposition of organic components and pyrolysis of the coke material. The results were consistent with the literature [41].

3.1.2 CdO-ESM Nanopowders

The TGA curve of the as-prepared CdO-ESM nanopowders is shown in Fig. 3a. The preliminary weight loss of 8%, observed at a temperature range of 0–110 °C is accountable for the elimination of adsorbed water molecules. The major weight loss of 44%, at 110–190 °C is due to the elimination of organic compounds from the ESM. The terminal weight loss of 19% was noted at a temperature range of about

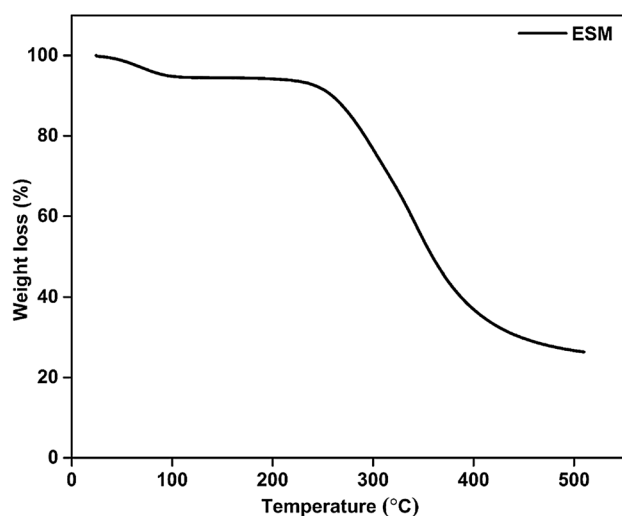


Fig. 2 TGA curve of dried ESM

190–510 °C, owing to the removal of carbonized products and the formation of CdO-ESM nanopowders. No weight loss remained above a temperature of 510 °C, hence demonstrating the thermal stability of CdO-ESM nanopowders. At this stage, the residual mass of CdO-ESM nanopowder was found to be 29%.

3.1.3 ZnO-ESM Nanopowders

The TGA curve of the as-prepared ZnO-ESM nanopowders curve is shown in Fig. 3b. The first weight loss of 7% was noted at a temperature range of 0–100 °C is accountable for the removal of water molecules from the surface of ESM. In addition to it, the elimination of organic components presents in the ESM caused another weight loss of 14% at 110–200 °C. Complete removal of coke content and formation of ZnO-ESM nanopowders led to yet another weight loss of 41%, at a temperature range of about 200–510 °C. No weight persisted above a temperature of 510 °C, hence establishing the thermal stability of ZnO-ESM nanopowders. At this stage, the residual mass of ZnO-ESM nanopowders was found to be 38%.

3.1.4 CdO/ZnO-ESM Nanocomposites

The TGA curve of the as-prepared CdO/ZnO-ESM nanocomposites are shown in Fig. 3c. The initial weight loss of 14%, observed at a temperature range of about 0–100 °C is accountable for the removal of water molecules (atmospheric moisture). The second weight loss of 9% at a temperature range of about 100–200 °C was attributed to the exclusion of organic elements from the ESM. Due to the complete removal of carbon content, the third weight loss of 41%, was detected at 200–510 °C. It is noted in the TGA curve that the ESM decomposes completely at about 510 °C or above. When no weight loss occurs as temperature increases, it means that the thermal stability of the prepared material up to 800 °C. At this stage, the residual mass of CdO/ZnO-ESM nanocomposites were found to be 36%.

3.2 Structural Analysis

The determination of the crystal structure of prepared CdO-ESM nanopowders, ZnO-ESM nanopowders, and CdO/ZnO-ESM nanocomposites using PXRD analysis are shown in Fig. 4a–c.

3.2.1 CdO-ESM Nanopowders

The PXRD pattern of CdO-ESM nanopowders has a diffraction peak at $2\theta = 33.05^\circ$, 38.38° , 55.31° , 65.97° and 69.29° with the plane values of (111), (200), (220), (311) and (222), respectively. The above peaks position

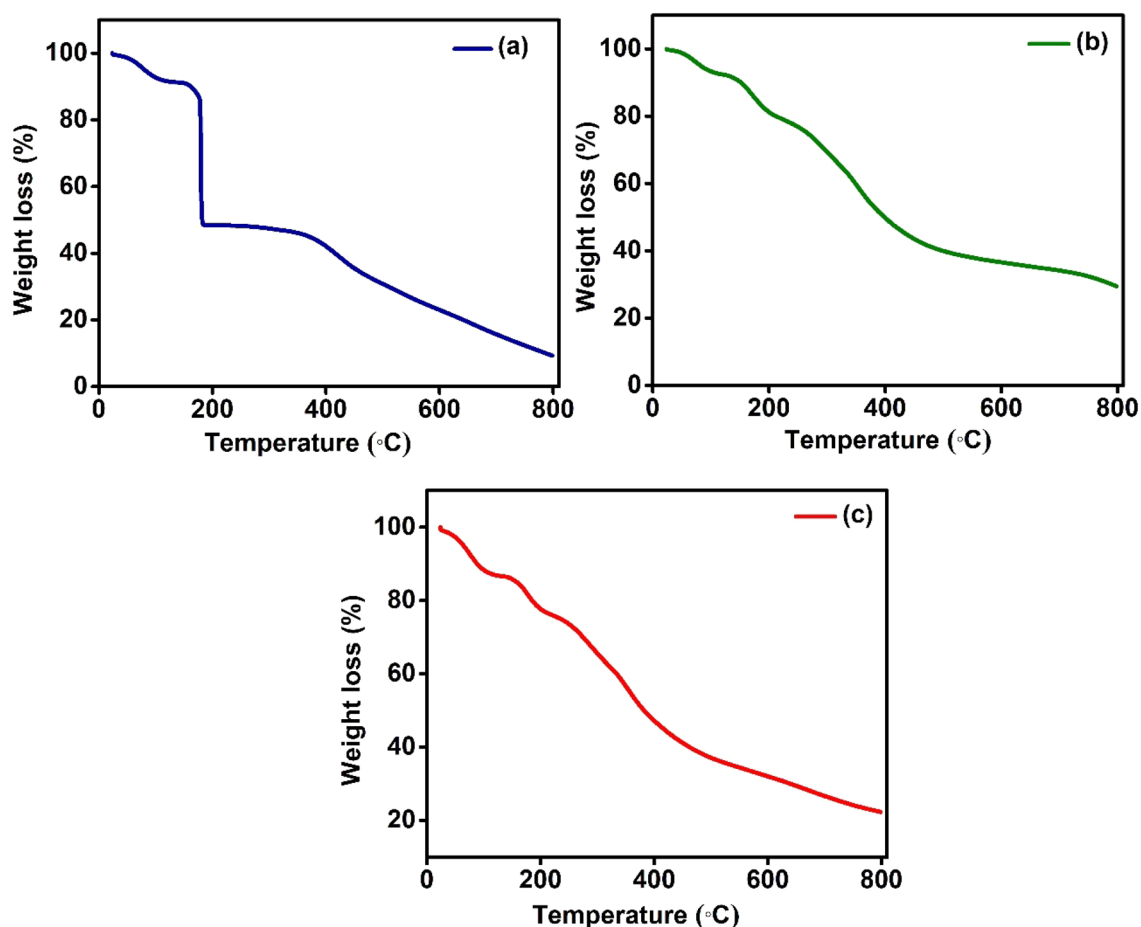


Fig. 3 TGA curve of as-prepared **a** CdO-ESM nanopowders, **b** ZnO-ESM nanopowders, **c** CdO/ZnO-ESM nanocomposites

corresponds to the single-phase cubic Montepelite structure with reference (JCPDS card no. 05-0640) and had matched with the earlier report [46]. The crystallite size has been calculated from the intense peak of whose plane values of (111) using Eq. (1). The obtained crystallite size was found to be 55.01 nm.

3.2.2 ZnO-ESM Nanopowders

The PXRD pattern of ZnO-ESM nanopowders confirms the formation of hexagonal ZnO with zincite structure according to (JCPDS card no. 36-1451). The diffraction peaks at $2\theta = 31.72^\circ, 34.37^\circ, 36.26^\circ, 47.54^\circ, 56.54^\circ, 62.80^\circ, 67.82^\circ$ and 69.05° corresponding to the plane values of (100), (002), (101), (102), (110), (103), (112) and (201), respectively. The above-mentioned results had matched the previous report [41]. The crystallite size has been calculated from the intense diffraction peak, whose plane values of (101) using Eq. (1). The obtained crystallite size was found to be 39.66 nm.

3.2.3 CdO/ZnO-ESM Nanocomposites

The PXRD pattern of CdO/ZnO-ESM nanocomposites contain the mixed phase of both CdO and ZnO. The results show the major peaks of hexagonal ZnO with zincite structure (JCPDS no. 36-1451). The diffraction peaks at 2θ values are $34.48^\circ, 36.21^\circ, 56.56^\circ, 62.85^\circ,$ and 67.91° which corresponds to the plane values of (002), (101), (110), (103) and (112) respectively. Also, minor peaks of CdO in cubic Montepelite (JCPDS no. 05-0640) phases with diffraction peaks at 2θ values are $32.86^\circ, 38.35^\circ,$ and 55.21° which corresponds to the plane values of (111), (200) and (220), respectively. The results are exactly matched with the earlier reports [41, 46]. The crystallite size was calculated using Eq. (1). The calculated crystallite size was found to 35.18 nm.

$$D = k\lambda/\beta \cos \theta \quad (1)$$

where, k —Scherrer's constant, λ —X-ray wavelength (1.5406 \AA), β —line broadening at half the maximum

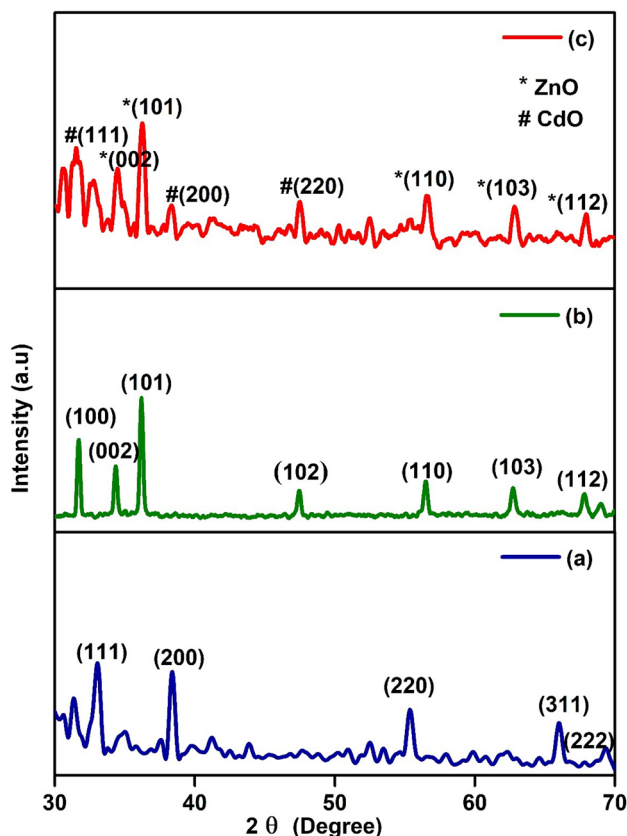


Fig. 4 PXRD Spectrum of **a** CdO-ESM nanopowders, **b** ZnO-ESM nanopowders, **c** CdO/ZnO-ESM nanocomposites

intensity (FWHM) in radians, θ —Bragg angle, and D —crystallite size.

3.3 Linear Optical Studies

The bandgap energy of semiconductor materials is measured using UV–Visible Diffuse Reflectance spectroscopy. Figure 5a–c shows the diffuse reflectance spectrum of CdO-ESM nanopowders, ZnO-ESM nanopowders, and CdO/ZnO-ESM nanocomposites within the range of wavelengths 200–800 nm.

3.3.1 CdO-ESM Nanopowders

The steep absorption band is observed at around 360–530 nm wavelength, corresponds to the bandgap energy of the CdO [47]. The absorption inflection point observed at 492 nm depicts the excitonic feature of CdO [48]. In this study of CdO-ESM nanopowders, the absorption inflection wavelength was noted to be 490 nm, and steep absorption was about 360–530 nm. The results matched with the previous reports [47, 48].

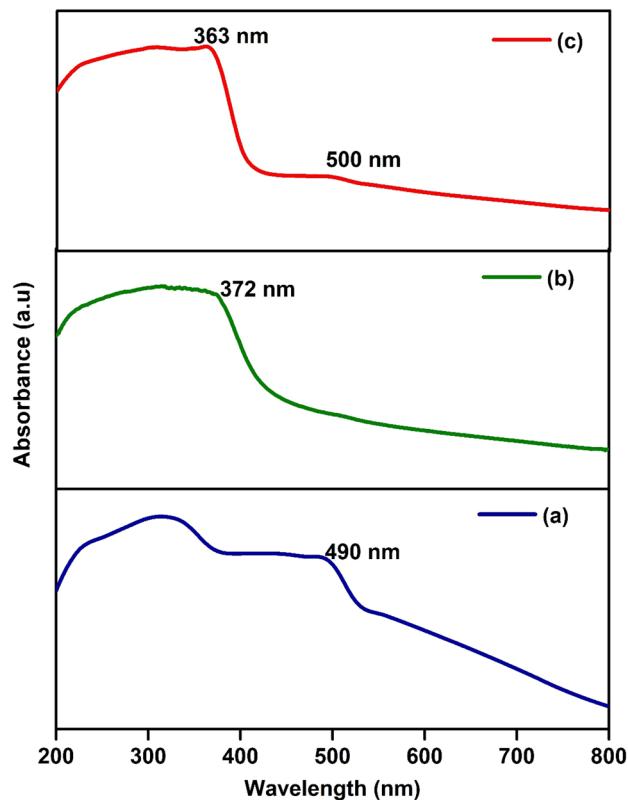


Fig. 5 Diffuse reflectance UV–Visible spectrum of **a** CdO-ESM nanopowders, **b** ZnO-ESM nanopowders, **c** CdO/ZnO-ESM nanocomposites

3.3.2 ZnO-ESM Nanopowders

The absorption band for ZnO-ESM nanopowders was observed at 372 nm is due to the presence of ZnO [49].

3.3.3 CdO/ZnO-ESM Nanocomposites

CdO/ZnO-ESM nanocomposites display two absorption edges at 363 nm and 510 nm is due to the presence of ZnO and CdO respectively. The wavelength towards blueshift shows slight deviations as to the value mentioned in the literature [49]. The shift in the wavelength towards the visible region from 490 to 510 nm is responsible for ZnO by combining with CdO. These results are well-correlated with the literature [13].

Tauc's equation is used to determine the bandgap energy of the prepared materials

$$(\alpha h\nu)^{1/n} = A(h\nu - E_g) \quad (2)$$

where, A —constant, α —absorption co-efficient, E_g —bandgap energy (eV), $h\nu$ —incident photon energy, and $n = 1/2$

and 2 for direct and indirect transitions respectively. The direct bandgap energy is evaluated from Tauc's plot with $(\alpha h\nu)^2$ versus $h\nu$, as depicted in Fig. 6a–c. The derived values of bandgap energy are 2.27 eV, 3.16 eV for CdO-ESM nanopowders and ZnO-ESM nanopowders, and 2.90 eV for CdO/ZnO-ESM nanocomposites [13, 19].

3.4 Functional Group Analysis

FT-IR analysis is used to determine the chemical bonds and functional groups present in the prepared CdO-ESM nanopowders, ZnO-ESM nanopowders, and CdO/ZnO-ESM nanocomposites, as shown in Fig. 7a–c.

3.4.1 CdO-ESM Nanopowders

FT-IR spectrum of CdO-ESM nanopowders is shown in Fig. 7a. The peak at 3451 cm^{-1} holds evidence of physically adsorbed water. Similarly, the peak at 2294 cm^{-1} holds evidence for the presence of atmospheric CO_2 in the sample. The peak observed at 1640 cm^{-1} is due to the vibration of interlayer water molecules. The peak obtained at 1105 cm^{-1}

is due to the stretching vibration absorption spectra of O–H [16]. The presence of an alkyl group (asymmetric C–H stretching) corresponds to the peak observed at 2932 cm^{-1} . Furthermore, the peak at 1445 cm^{-1} is attributed to the presence of carbonate minerals $-\text{CO}_3^{2-}$ [30]. The peak at 619 cm^{-1} corresponds to the formation of the Cd–O bond [12].

3.4.2 ZnO-ESM Nanopowders

FT-IR spectrum of ZnO-ESM nanopowders is shown in Fig. 7b. The peak at 3472 cm^{-1} holds evidence of physically adsorbed water. Similarly, the peak at 2341 cm^{-1} holds evidence for the presence of atmospheric CO_2 in the sample. The peak observed at 1620 cm^{-1} is due to the vibration of interlayer water molecules. The peak obtained at 1142 cm^{-1} is due to the stretching vibration absorption spectra of O–H [16]. The presence of an alkyl group (asymmetric C–H stretching) corresponds to the peak observed at 2922 cm^{-1} . Furthermore, the peak at 1435 cm^{-1} is attributed to the presence of carbonate

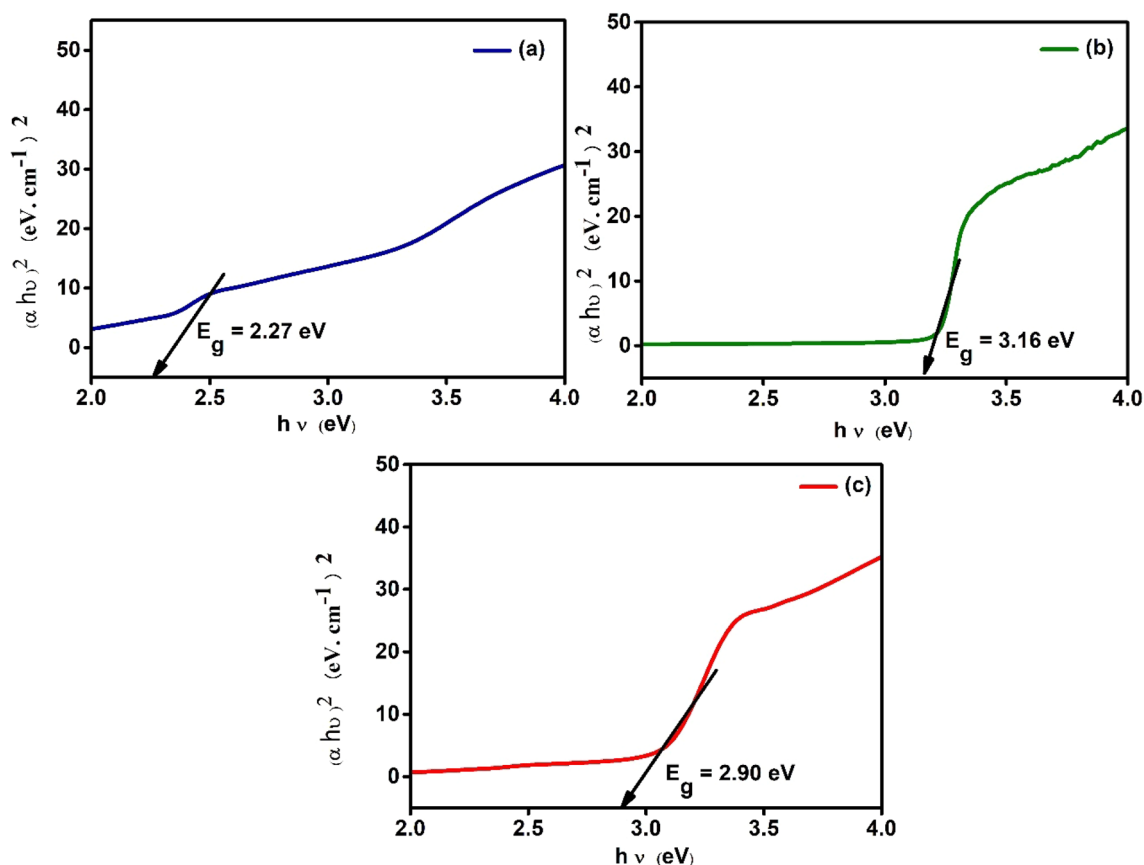


Fig. 6 Tauc's-plot analysis the direct band-gap transitions of **a** CdO-ESM nanopowders, **b** ZnO-ESM nanopowders, **c** CdO/ZnO-ESM nanocomposites

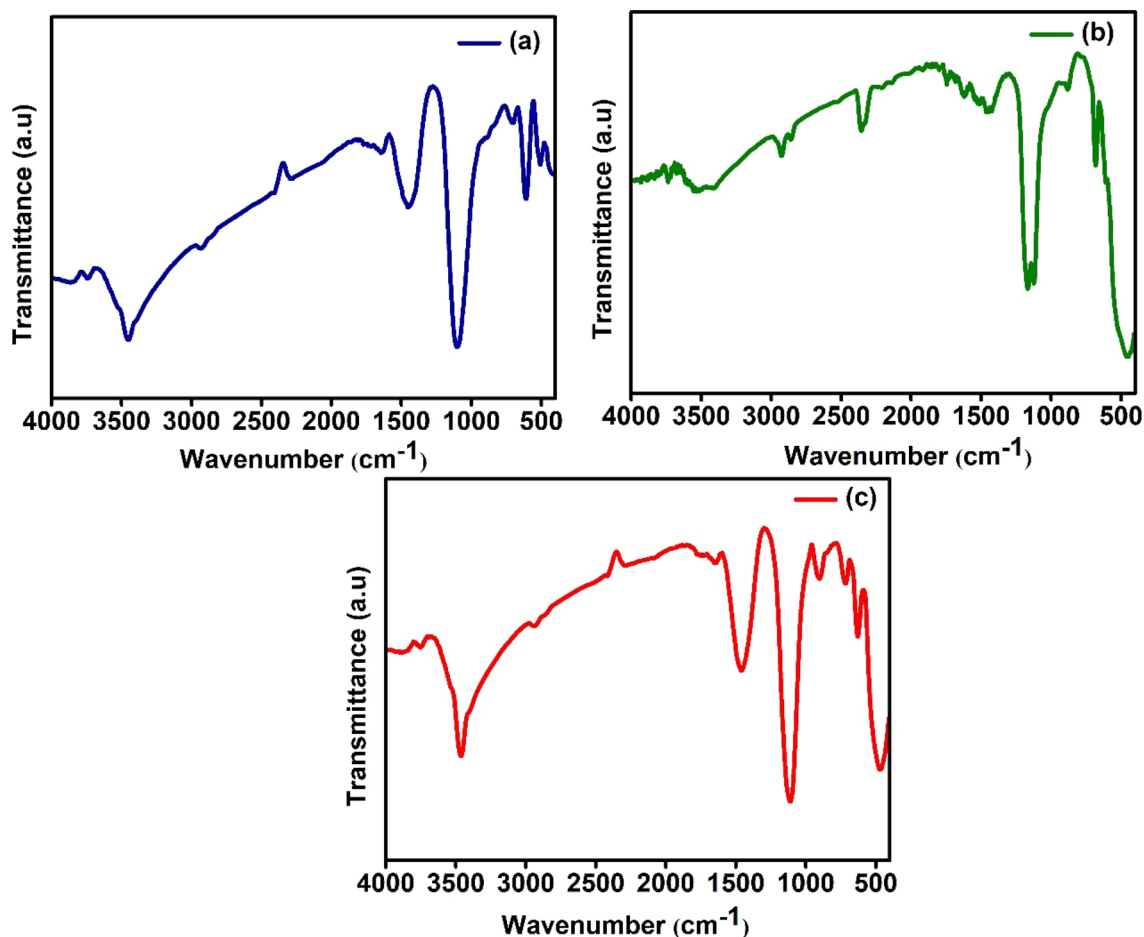


Fig. 7 FT-IR spectrum of **a** CdO-ESM nanopowders, **b** ZnO-ESM nanopowders, **c** CdO/ZnO-ESM nanocomposites

minerals CO_3^{2-} [30]. The peak at 444 cm^{-1} is due to the metal–oxygen stretching mode of ZnO [12].

3.4.3 CdO/ZnO-ESM Nanocomposites

FT-IR spectrum of CdO/ZnO-ESM nanocomposites are shown in Fig. 7c. The peak at 3446 cm^{-1} holds evidence of physically adsorbed water. Similarly, the peak at 2294 cm^{-1} holds evidence for the presence of atmospheric CO_2 in the sample. The peak observed at 1646 cm^{-1} is due to the vibration of interlayer water molecules. The peak obtained at 1110 cm^{-1} is due to the stretching vibration absorption spectra of O–H [16]. The presence of an alkyl group (asymmetric C–H stretching) corresponds to the peak observed at 2927 cm^{-1} . Furthermore, the peak at 1455 cm^{-1} is attributed to the presence of carbonate minerals CO_3^{2-} [30]. The peak at 462 cm^{-1} is due to the metal–oxygen stretching mode of ZnO and 627 cm^{-1} is due to the formation of the CdO bond [12].

3.5 Surface Morphology

SEM images of CdO-ESM nanopowders, ZnO-ESM nanopowders, and CdO/ZnO-ESM nanocomposites are illustrated in Fig. 8a–c. Figure 8a shows the surface morphology of CdO-ESM nanopowders appears flower-like structure along with rods. On the other hand, in Fig. 8b ZnO-ESM nanopowders show spherical shaped grains with aggregation. Figure 8c shows that CdO/ZnO-ESM nanocomposites exist both in flower-like structure and spherical grains, thereby indicating the presence of both CdO and ZnO.

3.6 EDAX Analysis

Figure 9a shows the EDAX spectrum of CdO-ESM nanopowders, a strong peak absorbed at 3–4 k eV corresponds to the presence of cadmium whereas oxygen detected within the range of 0.2–1 k eV. Therefore, the weight percentage of cadmium (56.91%) and oxygen (43.09%) respectively. Figure 9b shows the EDAX spectrum of ZnO-ESM

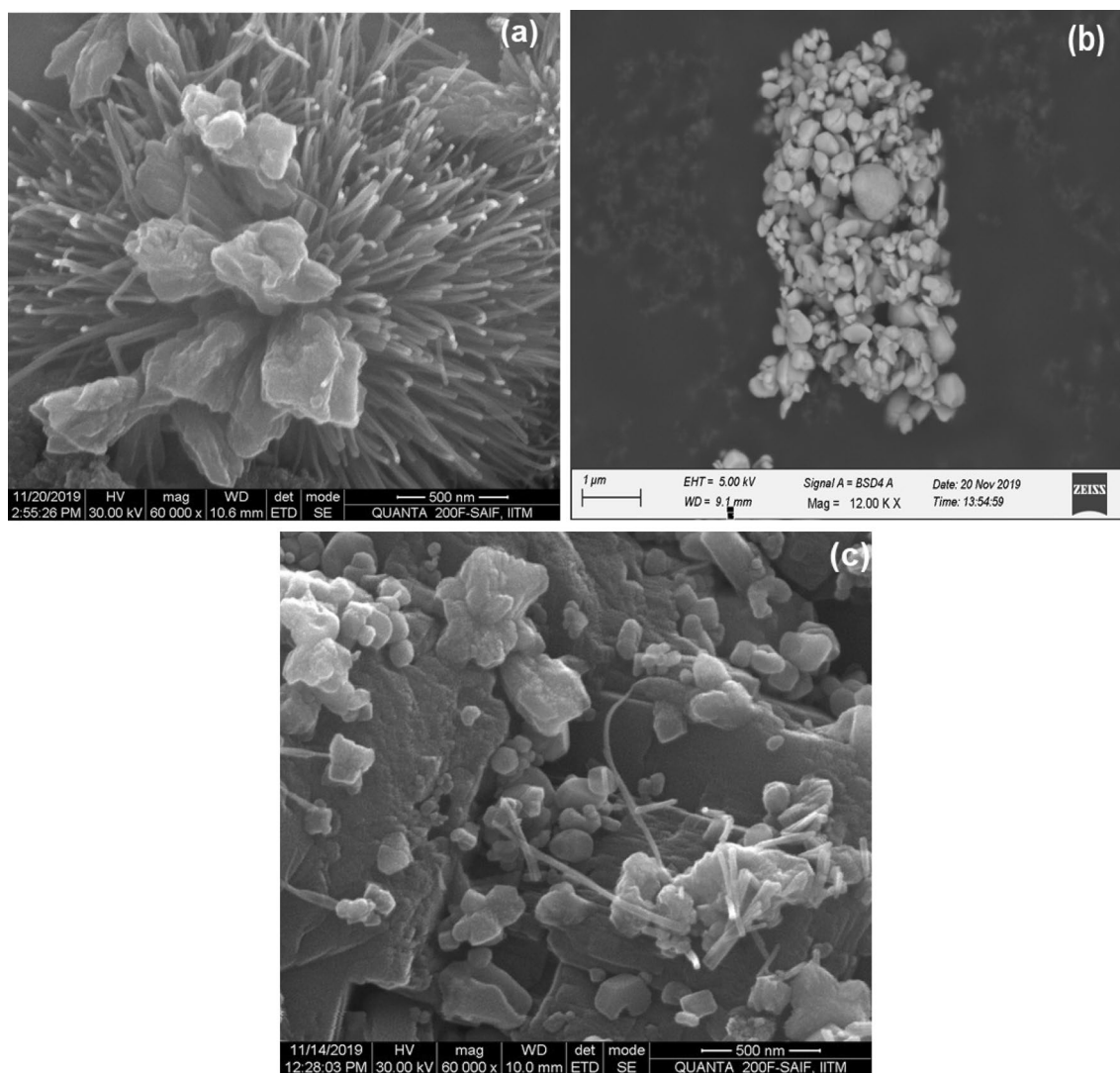


Fig. 8 SEM images of **a** CdO-ESM nanopowders, **b** ZnO-ESM nanopowders, **c** CdO/ZnO-ESM nanocomposites

nanopowders, a strong peak absorbed at 1.0 keV, and 9–10 keV corresponding to the presence of zinc whereas oxygen detected within the range of 0.2–0.5 keV. Therefore, the weight percentage of zinc and oxygen was noted to be 79.08% and 20.92% respectively. Figure 9c shows the EDAX spectrum of CdO/ZnO-ESM nanocomposites, a strong peak absorbed at 3–3.5 keV corresponding to the presence of cadmium whereas 1.0 keV, 8.8 keV, and 9.5 keV corresponding to the presence of zinc and oxygen detected in the range of 0.2–0.5 keV. Therefore, the weight percentage of cadmium (38.67%), zinc (42.13%), and oxygen (19.19%) respectively.

3.7 Investigation on Colloidal Properties

DLS-Zeta potential analysis was used to assess the stability of CdO-ESM nanopowders, ZnO-ESM nanopowders, and CdO/ZnO-ESM nanocomposites is depicted in Fig. 10a–c.

In accordance with the basic principle of the DLVO theory, high zeta potential value exerts a strong repulsive force between particles and prevents its aggregation [50]. In this analysis, negative zeta potential values for colloidal suspension of ZnO-ESM nanopowders and CdO/ZnO-ESM nanocomposites were -36.8 mV and -32.8 mV, indicating good stability and preventing aggregation of particles. For CdO-ESM nanopowders, the zeta potential value is lower, i.e. -21.8 mV, suggesting that there is no force to prevent the agglomeration and flocculation of the particles [51].

3.8 Photoluminescence Studies

Figure 11a–c shows the Photoluminescence spectrum of CdO-ESM nanopowders, ZnO-ESM nanopowders, and CdO/ZnO-ESM nanocomposites were analyzed at room temperature. The emission peak for CdO-ESM nanopowders

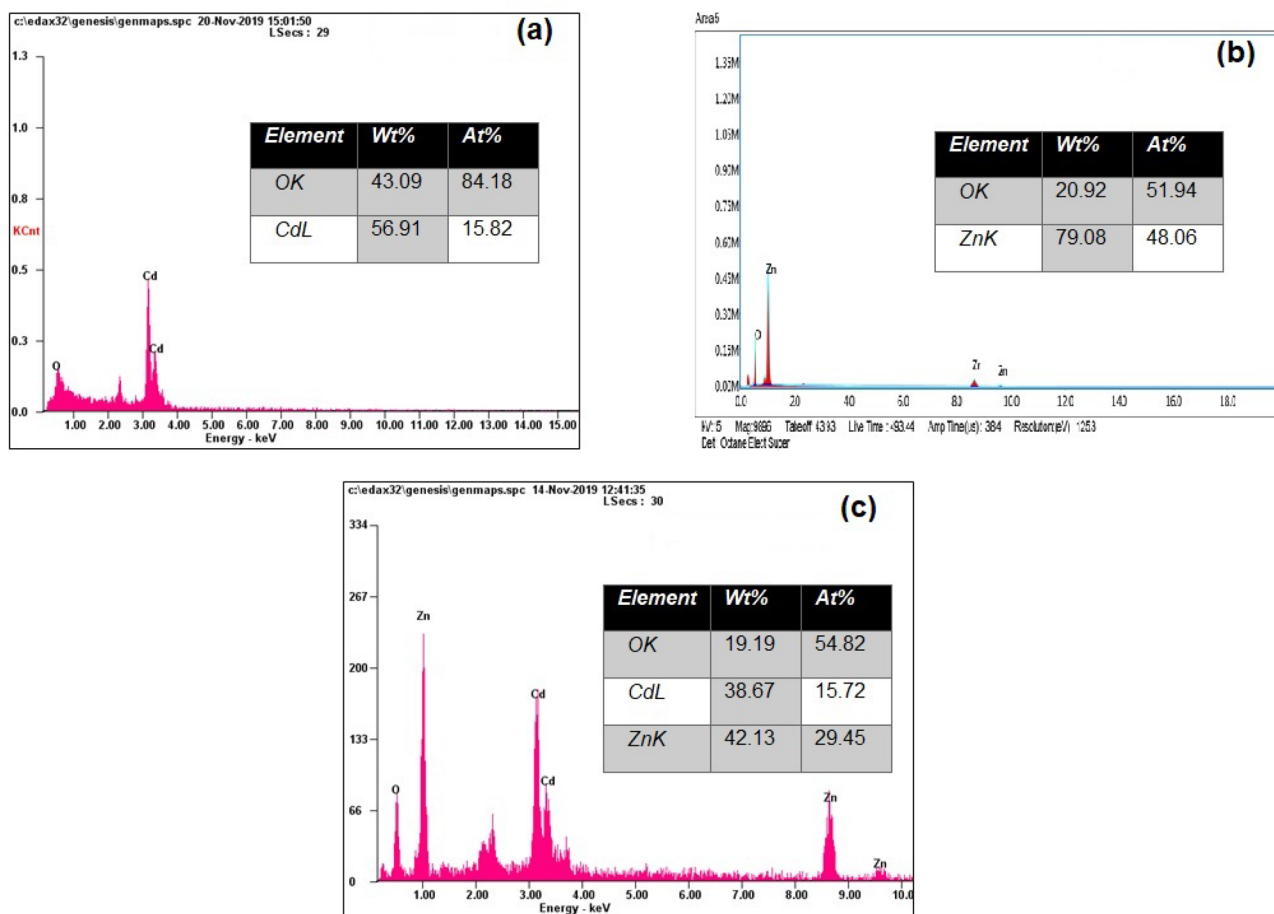


Fig. 9 EDAX spectrum of **a** CdO-ESM nanopowders, **b** ZnO-ESM nanopowders, **c** CdO/ZnO-ESM nanocomposites

is 496 nm, while the emission peak for ZnO-ESM nanopowders is 571 nm. For CdO/ZnO-ESM nanocomposites, due to quantum confinement, the emission peaks shifted slightly to the lower wavelength at 494 nm and 566 nm and also the peaks occurred at 496 and 494 nm is attributed to the transition from Zn interstitials (Zn_i) to the valence band and therefore the peak at 494 nm could also be the results of the singly ionized oxygen vacancy (V_o). Additional peaks observed at 523 nm for ZnO-ESM and 520 nm for CdO/ZnO-ESM nanocomposites are attributable to the recombination of photogenerated holes with a single ionized state of charge with a specific defect. These values are in good agreement with the reported literature [13].

3.9 Antimicrobial Activity

The antimicrobial activity of CdO-ESM nanopowders, ZnO-ESM nanopowders, and CdO/ZnO-ESM nanocomposites were tested against both Gram-positive and Gram-negative bacteria by agar well diffusion method.

3.9.1 CdO-ESM Nanopowders

The antimicrobial activity of CdO-ESM nanopowders was tested at a concentration of 30 $\mu\text{g/mL}$. The Petri-plates photographic images were shown in Fig. 12 and therefore the zone of inhibition values was measured in diameter (mm) are revealed in Table 2. The maximum zone of inhibition was observed in *Bacillus* sp. (24 mm) followed by *Staphylococcus aureus* (23 mm), *Klebsiella pneumonia* (23 mm), *Salmonella enterica* (23 mm), *Pseudomonas aeruginosa* (21 mm), *Escherichia coli* (18 mm) and *Vibrio* sp. (17 mm) respectively.

3.9.2 ZnO-ESM Nanopowders

The antimicrobial activity of ZnO-ESM nanopowders was tested at a concentration of 30 $\mu\text{g/mL}$. The Petri-plates photographic images are shown in Fig. 12 and the zone of inhibition values measured in diameter (mm) are mentioned in Table 2. The maximum zone of inhibition was observed in *Bacillus* sp. (23 mm) followed

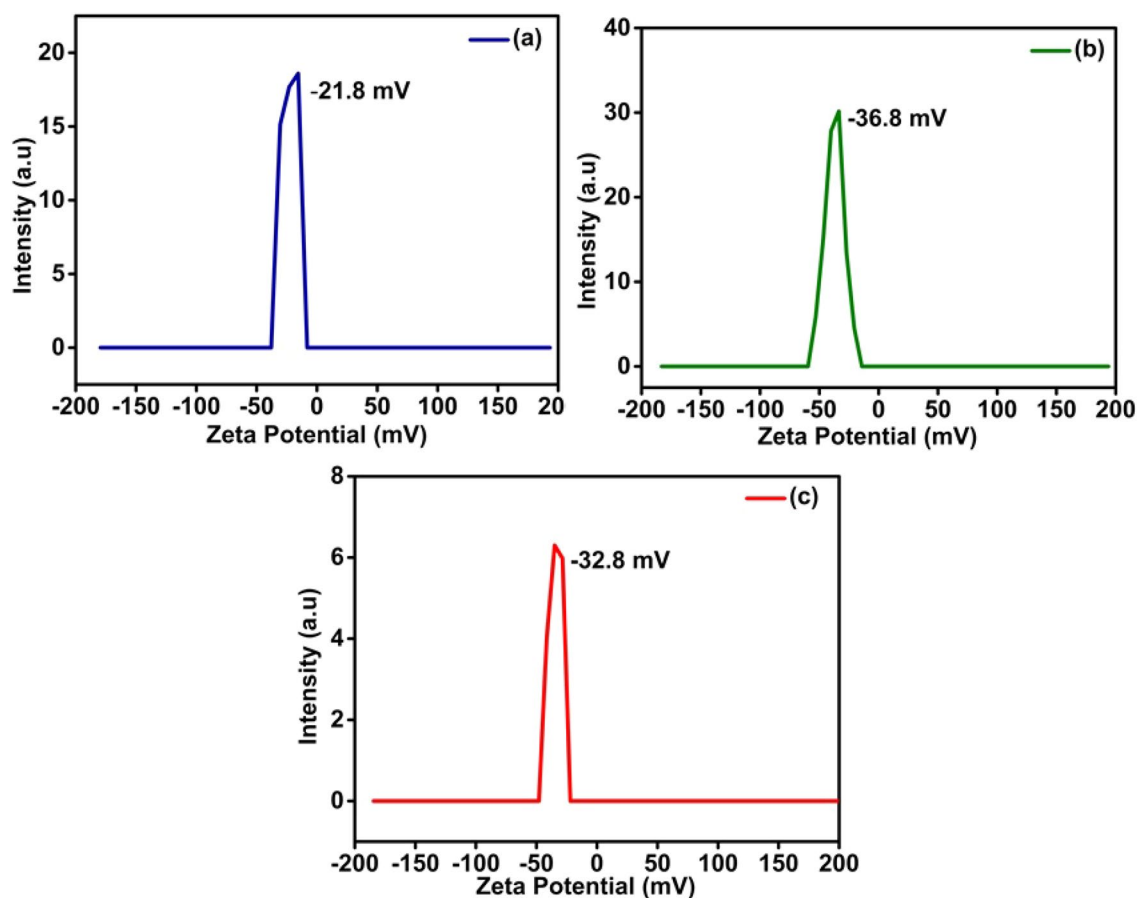


Fig. 10 Zeta potential analysis of **a** CdO-ESM nanopowders, **b** ZnO-ESM nanopowders, **c** CdO/ZnO-ESM nanocomposites

by *Salmonella enterica* (22 mm), *Klebsiella pneumonia* (21 mm), *Escherichia coli* (20 mm), *Staphylococcus* and *Pseudomonas aeruginosa* (19 mm) and *Vibrio* sp. (17 mm) respectively.

3.9.3 CdO/ZnO-ESM Nanocomposites

The antimicrobial activity of CdO/ZnO-ESM nanocomposites were tested at a concentration of 30 $\mu\text{g}/\text{mL}$. The Petri-plates photographic images were shown in Fig. 12 and the zone of inhibition values were measured in diameter (mm) are stated in Table 2. The maximum zone of inhibition was observed in *Salmonella enterica* (24 mm) followed by *Staphylococcus aureus* (20 mm), *Bacillus* sp. (20 mm), *Escherichia coli* (20 mm) and *Vibrio* sp. (20 mm), *Klebsiella pneumonia* (19 mm) and *Pseudomonas aeruginosa* (18 mm) respectively. The above results showed good antimicrobial activity and the zone of inhibition was merely the same for all the prepared samples.

3.9.4 Mechanism of Antimicrobial Activity

The antimicrobial activity of ESM assisted with the synthesis of CdO-ESM nanopowders, ZnO-ESM nanopowders, and CdO/ZnO-ESM nanocomposites were tested against both Gram-positive bacteria (*Staphylococcus aureus* and *Bacillus* sp.) and Gram-negative bacteria (*Escherichia coli*, *Klebsiella pneumonia*, *Pseudomonas aeruginosa*, *Salmonella enterica*, and *Vibrio* sp.). The antimicrobial activity of ZnO nanoparticles has four major concepts of mechanisms: (i) generation of ROS by UV or visible light illumination (ii) releasing metal ions by irradiation, i.e. photo-dissolution, or photo corrosion (iii) membrane dysfunction and (iv) nanoparticle internalization [52].

In this work, the generation of reactive oxygen species and the release of metal ions are not possible because this experiment was performed in the laboratory environment conditions. The mechanism of the antimicrobial activity in the present work might be membrane dysfunction or nanoparticle internalization. Generally, the Gram-positive bacterial cell wall consists of thick, dense peptidoglycan

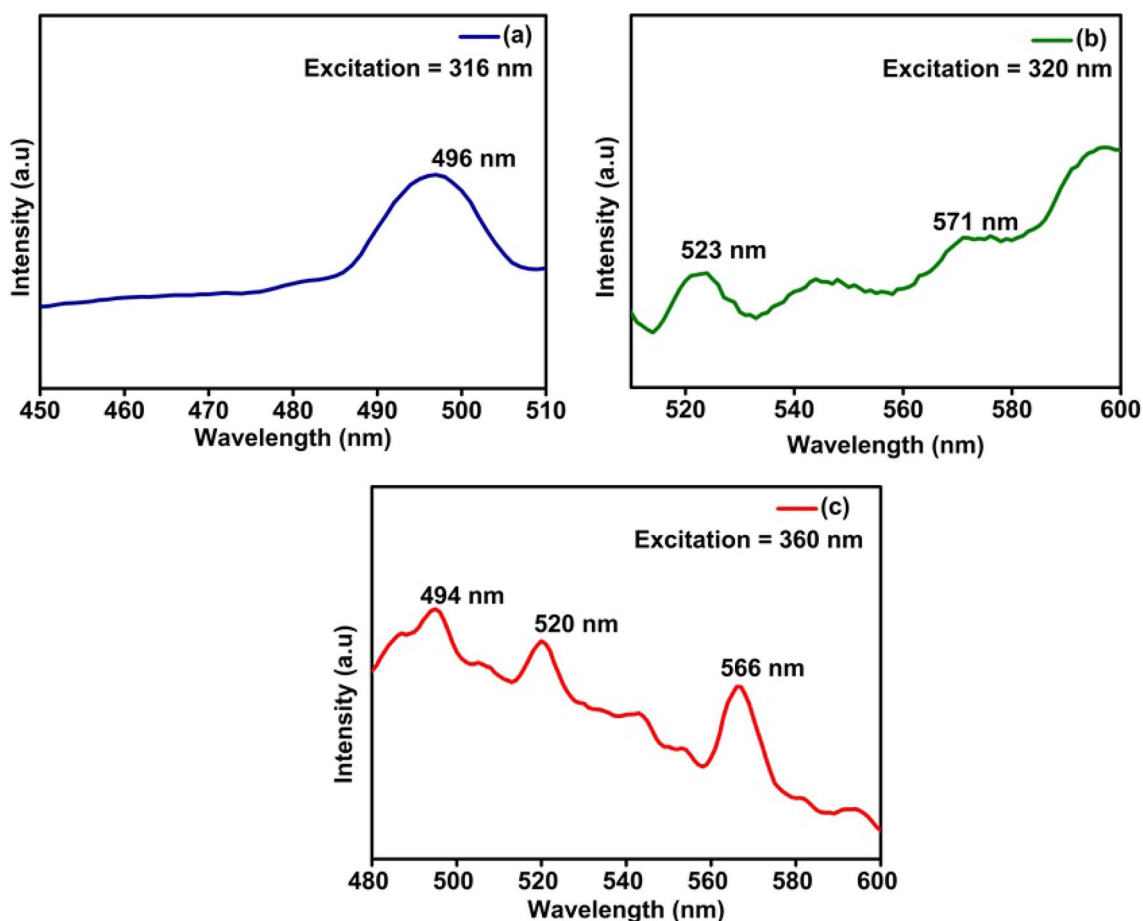


Fig. 11 Photoluminescence spectrum of **a** CdO-ESM nanoparticles, **b** ZnO-ESM nanoparticles, **c** CdO/ZnO-ESM nanocomposites

and teichoic acid. The Gram-negative bacteria, on the other hand, are made of three layers. The outer layer is made up of protein matrix, fat, phospholipids, and lipopolysaccharides. The middle layer is made out of peptidoglycan. The inner layer is made up of phospholipids and protein. Both types of bacteria have a negatively charged cell surface.

In this work, positively charged CdO/ZnO-ESM nanocomposites can come into contact with a negatively charged bacterial cell surface that attracts each other by electrostatic interactions. As a result, the charge balance on the surface causes the cell to deform seriously and kill bacteria. On the other hand, the CdO/ZnO-ESM nanocomposites internalize bacteria, thereby inhibiting and shutting down the vital and vulnerable exchange of matter and energy metabolism in the bacterial environment. After CdO/ZnO-ESM nanocomposites have destroyed and disintegrated the cell membrane, they are internalized into the bacteria. Disturbing the membrane can lead to loss of membrane integrity which can lead to failure

of the permeability barrier. A similar mechanism has been applied to CdO-ESM nanoparticles and ZnO-ESM nanoparticles.

3.9.5 MIC Value of Antimicrobial Activity

MIC value provide quantitative data on the antimicrobial efficiency of CdO-ESM nanoparticles, ZnO-ESM nanoparticles, and CdO/ZnO-ESM nanocomposites were tested against both Gram-positive and Gram-negative bacteria by Resazurin-based microdilution assay.

3.9.5.1 CdO-ESM Nanopowders The different concentrations of CdO-ESM nanoparticles (1000–0.49 $\mu\text{g/mL}$) were tested and are shown in Fig. 13. The MIC values are shown in Table 3. The MIC values of CdO-ESM nanopowder was high in 0.98 ($\mu\text{g/mL}$) for *Bacillus* sp. and *Klebsiella pneumoniae*, 1.95 ($\mu\text{g/mL}$) for *Salmonella enterica*, 7.81 ($\mu\text{g/mL}$) for *Staphylococcus aureus* and *Pseudomonas aeruginosa*, 15.6 ($\mu\text{g/mL}$) for *Vibrio* sp. and 31.25 ($\mu\text{g/mL}$) for *Escherichia coli*.

Fig. 12 Antimicrobial activity of (a) CdO-ESM nanopowders, (b) ZnO-ESM nanopowders, (c) CdO/ZnO-ESM nanocomposites, (d) negative control (50 mM; pH 5.0; sodium acetate buffer solution), (e) positive control (15 µg/mL Streptomycin) against test microorganisms

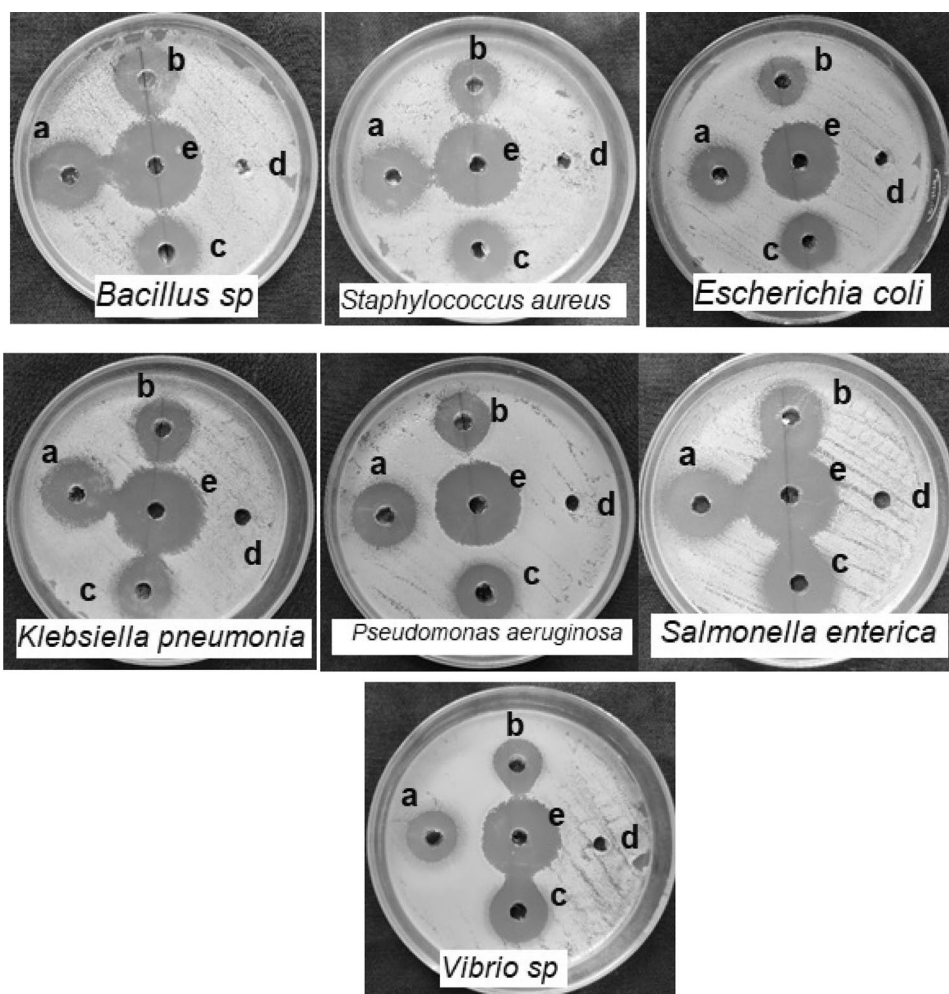


Table 2 Antimicrobial activity of CdO-ESM nanopowders, ZnO-ESM nanopowders and CdO/ZnO-ESM nanocomposites against test microorganisms

Test microorganisms	Zone of inhibition (mm) ^a				
	CdO-ESM nanopowders	ZnO-ESM nanopowders	CdO/ZnO-ESM nanocomposites	NC	PC
Gram-positive bacteria					
<i>Staphylococcus aureus</i>	23	19	20	–	29
<i>Bacillus sp.</i>	24	23	20	–	29
Gram-negative bacteria					
<i>Escherichia coli</i>	18	20	20	–	29
<i>Klebsiella pneumonia</i>	23	21	19	–	30
<i>Pseudomonas aeruginosa</i>	21	19	18	–	27
<i>Salmonella enterica</i>	23	22	24	–	28
<i>Vibrio sp.</i>	17	17	20	–	28

(–) no activity, NC negative control (50 mM; pH 5.0 sodium acetate buffer solution), PC positive control (15 µg/mL Streptomycin)

^aDiameter (mm)—zone of inhibition (including the disc diameter (6 mm))

3.9.5.2 ZnO-ESM Nanopowders The different concentrations of ZnO-ESM nanopowders (1000–0.49 µg/mL) were tested and are shown in Fig. 13. The MIC values are shown

in Table 3. The MIC values of ZnO-ESM nanopowders was high in 1.95 (µg/mL) for *Bacillus sp.*, *Klebsiella pneumonia* and *Salmonella enterica*, 7.81 (µg/mL) for *Staphylococ-*

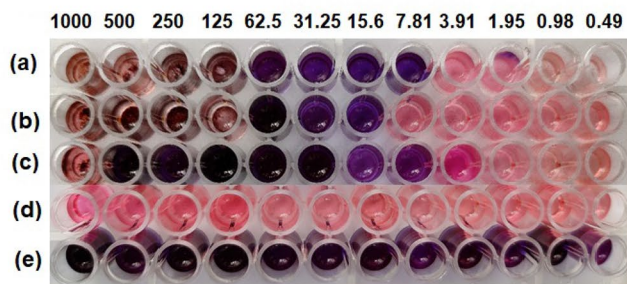
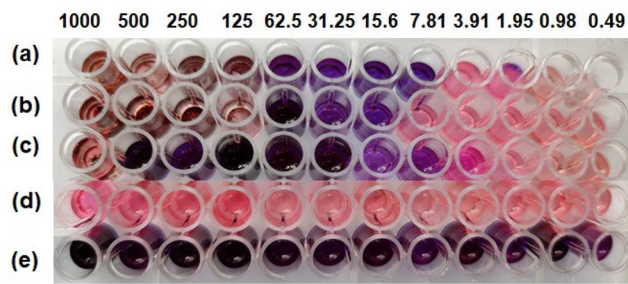
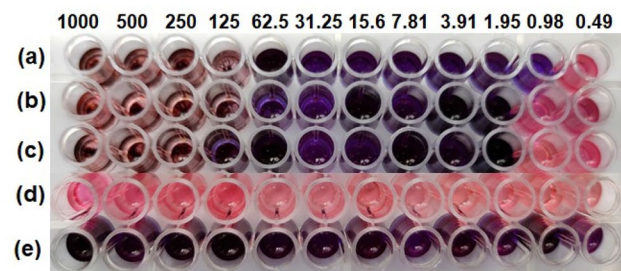
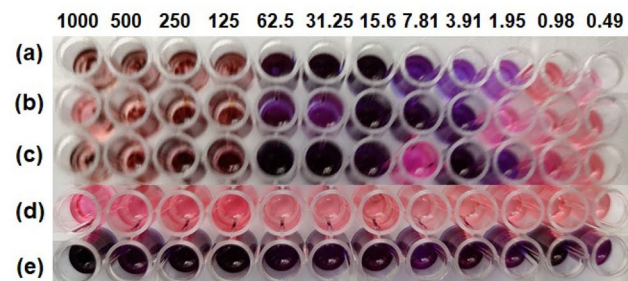
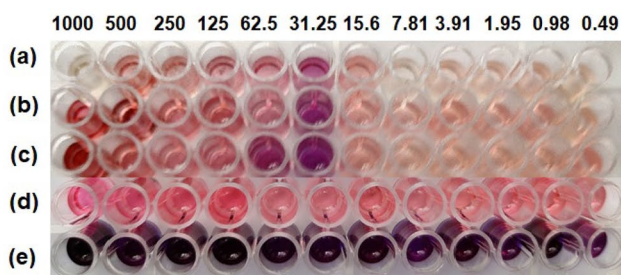
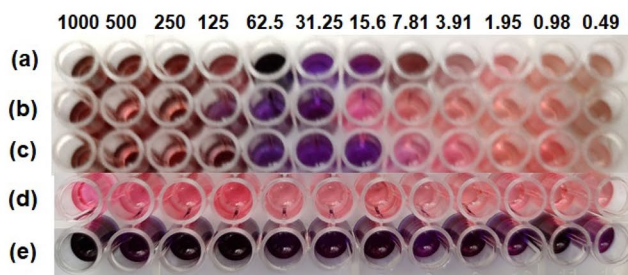
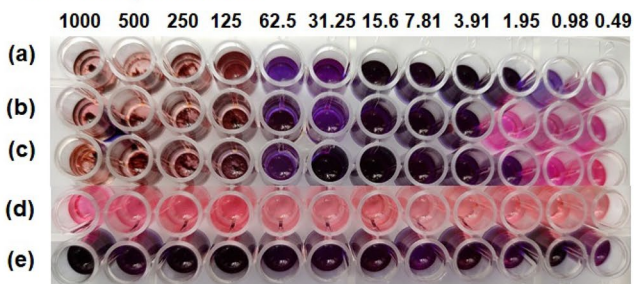
Staphylococcus aureus***Pseudomonas aeruginosa******Bacillus sp******Salmonella enterica******Escherichia coli******Vibrio sp******Klebsiella pneumonia***

Fig. 13 Photographic images of MIC values of (a) CdO-ESM nanopowders, (b) CdO/ZnO-ESM nanocomposites, (c) ZnO-ESM nanopowders, (d) negative control (50 mM; pH 5.0 sodium acetate buffer), (e) positive control (streptomycin 15 $\mu\text{g}/\text{mL}$) against test microorganisms

cus aureus and *Pseudomonas aeruginosa*, 15.6 ($\mu\text{g}/\text{mL}$) for *Vibrio sp.* and 31.25 ($\mu\text{g}/\text{mL}$) for *Escherichia coli*.

3.9.5.3 CdO/ZnO-ESM Nanocomposites The different concentrations of CdO/ZnO-ESM composites (1000–0.49 $\mu\text{g}/\text{mL}$) were tested and are shown in Fig. 13. The MIC values are shown in Table 3. The MIC values of

CdO/ZnO-ESM nanocomposites were high in 1.95 ($\mu\text{g}/\text{mL}$) for *Bacillus sp.*, 3.91 ($\mu\text{g}/\text{mL}$) for *Klebsiella pneumonia* and *Salmonella enterica*, 15.6 ($\mu\text{g}/\text{mL}$) for *Staphylococcus aureus* and *Pseudomonas aeruginosa*, 31.25 ($\mu\text{g}/\text{mL}$) for *Vibrio sp.* and *Escherichia coli*.

Table 3 Minimum inhibitory concentration of CdO-ESM nanopowders, ZnO-ESM nanopowders and CdO/ZnO-ESM nanocomposites against test microorganisms

Test microorganisms	Minimum inhibitory concentration ($\mu\text{g/mL}$)				
	CdO-ESM nanopowders	ZnO-ESM nanopowders	CdO/ZnO-ESM nanocomposites	NC	PC
Gram-positive bacteria					
<i>Staphylococcus aureus</i>	7.81	7.81	15.6	–	0.49
<i>Bacillus</i> sp.	0.98	1.95	1.95	–	0.49
Gram-negative bacteria					
<i>Escherichia coli</i>	31.25	31.25	31.25	–	0.49
<i>Klebsiella pneumonia</i>	0.98	1.95	3.91	–	0.49
<i>Pseudomonas aeruginosa</i>	7.81	7.81	15.6	–	0.49
<i>Salmonella enterica</i>	1.95	1.95	3.91	–	0.49
<i>Vibrio</i> sp.	15.6	15.6	31.25	–	0.49

PC positive control (15 $\mu\text{g/mL}$ streptomycin), (–) no activity, NC negative control (50 mM; pH 5.0 sodium acetate buffer solution)

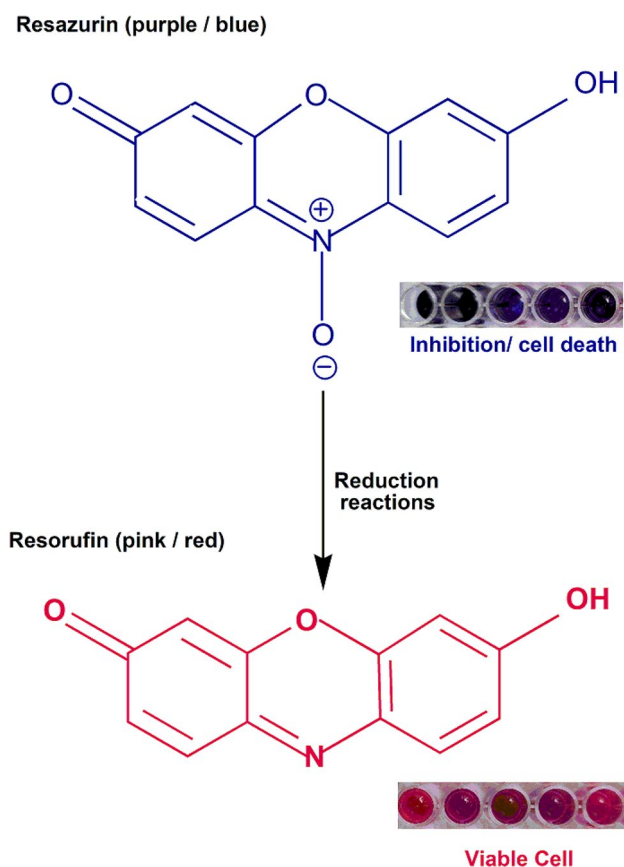


Fig. 14 The mechanism of minimum inhibitory concentration using resazurin-based (broth microdilution method)

3.9.5.4 Mechanism of MIC Resazurin, a redox-sensitive dye used to indicate cell viability. Metabolically active cells reduce non-fluorescent (blue/purple) resazurin to fluorescent (pink/red) resorufin. The presence of viable cells in the well produces oxidoreductase enzyme, which

can reduce resazurin into resorufin. This visible change in color to fluorescence (pink/red) indicates that cells are viable. Non-Fluorescent (blue/purple) indicates cell death or inhibition of bacterial cell wall [45]. Based on this observation, the MIC values of both Gram-positive and Gram-negative bacteria were fixed. The mechanism of minimum inhibitory concentration using resazurin-based (broth microdilution method) is shown in Fig. 14.

3.9.6 Comparison of the Antimicrobial Activity Efficiency of CdO/ZnO Nanocomposites Against Both Gram-Positive and Gram-Negative Bacteria

In the previous study, few reports are reported of CdO/ZnO nanocomposites as an antimicrobial agent for both Gram-positive and Gram-negative bacteria. Table 4 summarizes the literature on antimicrobial activity of CdO/ZnO nanocomposites, which uses various methods such as microwave-assisted, thermal treatment, magnetron sputtering and Honey assisted combustion method. Inhibition zone (mm) and MIC value ($\mu\text{g/mL}$) of CdO/ZnO nanocomposites are observed to be higher or lower than previous studies. In comparison with the above-mentioned methods, eggshell membrane-mediated synthesis of CdO/ZnO-ESM nanocomposites are simple, non-toxic, eco-friendly, and cost-effective.

4 Conclusion

In this study, CdO/ZnO-ESM nanocomposites have been successfully synthesized by using ESM as a bio-template, reducing, and stabilizing agents. The antimicrobial activity of prepared CdO/ZnO-ESM nanocomposites was tested

Table 4 Comparison of the antimicrobial activity efficiency of CdO/ZnO nanocomposites against test microorganisms

Test microorganisms	Material	Zone of inhibition (mm)	Concentration ($\mu\text{g/mL}$)	References
<i>Staphylococcus aureus</i>	CdO/ZnO	–	–	[10]
		12	80	[5]
		40 ± 0.6	10	[11]
		31	100	[25]
		20	30	Present study
<i>Bacillus</i> sp.	CdO/ZnO	9 ± 0.4	10	[10]
		10	80	[5]
		36 ± 0.6	15	[11]
		26	100	[25]
		20	30	Present study
<i>Escherichia coli</i>	CdO/ZnO	8	10	[10]
		18	80	[5]
		39 ± 0.8	10	[11]
		14	100	[25]
		20	30	Present study
<i>Klebsiella pneumonia</i>	CdO/ZnO	–	–	[10]
		14	80	[5]
		33 ± 0.8	20	[11]
		–	–	[25]
		19	30	Present study
<i>Pseudomonas aeruginosa</i>	CdO/ZnO	–	–	[10]
		–	–	[5]
		36 ± 0.6	15	[11]
		–	–	[25]
		18	30	Present study
<i>Salmonella enterica</i>	CdO/ZnO	–	–	[10]
		13	80	[5]
		–	–	[11]
		–	–	[25]
		24	30	Present study
<i>Vibrio</i> sp.	CdO/ZnO	–	–	[10]
		–	–	[5]
		–	–	[11]
		–	–	[25]
		20	30	Present study

against both Gram-positive and Gram-negative bacteria. The MIC values were concomitantly determined. The zone of inhibition indicates to be good even at a low concentration (30 $\mu\text{g/mL}$) of CdO/ZnO-ESM nanocomposites. Substantial MIC values were also obtained. It is therefore concluded that the pathway mentioned in this paper for the preparation of CdO/ZnO-ESM nanocomposites are simple, environmentally friendly, non-toxic, and cost-effective. Therefore, the prepared CdO/ZnO-ESM nanocomposites may potentially be used as antimicrobial agents for the treatment of assorted bacterial diseases. Future work on

CdO/ZnO-ESM nanocomposites for the photocatalytic degradation of contaminants will also be encouraging.

Acknowledgements The author, Dr. K. Venkatachalam gratefully acknowledges the financial assistance from the Department of Science and Technology, India for the DST-SERB Project (Ref. No. EEQ/2016/000559, Date.: 06.02.2017).

Author contributions PSSS—conceptualization; methodology; formal analysis; investigation; writing original draft preparation; writing-review and editing. GSC—investigation and methodology. DG—data curation. PP—providing laboratory for testing antimicrobial activity. VK—funding acquisition; visualization; supervision and project administration.

Compliance with Ethical Standards

Conflict of interest The authors report no declarations of interest.

References

1. A. Azam, A.S. Ahmed, M. Oves, M.S. Khan, S.S. Habib, A. Memic, Antimicrobial activity of metal oxide nanoparticles against Gram-positive and Gram-negative bacteria: a comparative study. *Int. J. Nanomed.* **7**, 6003–6009 (2012). <https://doi.org/10.2147/ijn.s35347>
2. V. Stanic, S.B. Tanaskovic, Antibacterial activity of metal oxide nanoparticles. *Nanotoxicity* **11**, 241–274 (2020). <https://doi.org/10.1016/B978-0-12-819943-5.00011-7>
3. R. Kumar, A. Umar, G. Kumar, H.S. Nalwa, Antimicrobial properties of nanomaterials: a review. *Ceram. Int.* **43**, 3940–3961 (2017). <https://doi.org/10.1016/j.ceramint.2016.12.062>
4. K. Kannan, D. Radhika, K.K. Sadasivuni, K. Raghava-Reddy, A.V. Raghunath, Nanostructured metal oxides and its hybrids for biomedical applications. *Adv. Coll. Interface. Sci.* **281**, 102178 (2020). <https://doi.org/10.1016/j.cis.2020.102178>
5. S. Cheemadan, M. Krishnan, A.J. Rathinam, M.C.S. Kumar, Biocidal properties of sputtered CdO:ZnO multi-component thin films for potential use in pathogenic bacteria control. *Mater. Res. Express* **6**, 104009 (2019). <https://doi.org/10.1088/2053-1591/ab3cbe>
6. E. Khalili, S.A. Hassanzadeh Tabrizi, ZnO-CdO nanocomposite: microemulsion synthesis and dye removal ability. *J. Sol-Gel Sci. Technol.* **81**, 475–482 (2016). <https://doi.org/10.1007/s10971-016-4211-0>
7. A.H. Hateem, T. Ekhlass, W.M. Mohammed, M.M. Saleh, Green synthesis of CdO nanoparticles by olive leaf extract and their biological effectiveness. *Res. J. Chem. Environ.* **23**(1), 138–141 (2019)
8. T.V.M. Sreekanth, M. Pandurangan, G.R. Dillip, D.H. Kim, Y.R. Lee, Toxicity and efficacy of CdO nanostructures on the MDCK and Caki-2cells. *J. Photochem. Photobiol. B* **164**, 174–181 (2016). <https://doi.org/10.1016/j.jphotobiol.2016.09.028>
9. T. Bhuyan, K. Mishra, M. Khanuja, R. Prasad, A. Varma, Biosynthesis of zinc oxide nanoparticles from *Azadirachta indica* for antibacterial and photocatalytic applications. *Mater. Sci. Semicond. Process.* **32**, 55–61 (2015). <https://doi.org/10.1016/j.mssp.2014.12.053>
10. N.M. Al-Hada, H. Mohamed Kamari, C.A.C. Abdullah, E. Saion, A.H. Shaari, Z.A. Talib, K.A. Matori, Down-top nanofabrication of binary (CdO)_x(ZnO)_{1-x} nanoparticles and their antibacterial Activity. *Int. J. Nanomed.* **12**, 8309–8323 (2017). <https://doi.org/10.2147/IJN.S150405>
11. K. Karthik, S. Dhanuskodi, C. Gobinath, S. Sivaramkrishnan, Microwave-assisted synthesis of CdO-ZnO nanocomposite and its antibacterial activity against human pathogens. *Spectrochim. Acta A* **139**, 7–12 (2014). <https://doi.org/10.1016/j.saa.2014.11.079>
12. E. Mosquera, I. del Pozo, M. Morel, Structure and red shift of optical band gap in CdO-ZnO nanocomposite synthesized by the sol gel method. *J. Solid-State Chem.* **206**, 265–271 (2013). <https://doi.org/10.1016/j.jssc.2013.08.025>
13. C.V. Reddy, B. Babu, J. Shim, Synthesis, optical properties and efficient photocatalytic activity of CdO/ZnO hybrid nanocomposite. *J. Phys. Chem. Solids* **112**, 20–28 (2018). <https://doi.org/10.1016/j.jpcs.2017.09.003>
14. S. Rajaboopathi, S. Thambidurai, Green synthesis of seaweed surfactant based CdO-ZnO nanoparticles for better thermal and photocatalytic activity. *Curr. Appl. Phys.* **17**(12), 1622–1638 (2017). <https://doi.org/10.1016/j.cap.2017.09.006>
15. M.M. Raman, S.B. Khan, H.M. Marwani, A.M. Asiri, K.A. Alarmy, M.A. Rub, A. Khan, A.A.P. Khan, N. Azum, Facile synthesis of doped ZnO-CdO nanotubes as solid phase adsorbent and efficient solar photo-catalyst applications. *J. Ind. Eng. Chem.* **20**(4), 1622–1638 (2013). <https://doi.org/10.1016/j.jiec.2013.09.059>
16. P. Margan, M. Haghghi, Sono-coprecipitation synthesis and physicochemical characterization of CdO-ZnO nanophotocatalyst for removal of acid orange 7 from wastewater. *Ultrason. Sonochem.* **40**, 323–332 (2017). <https://doi.org/10.1016/j.ultsonch.2017.07.003>
17. M. Mahendiran, J.J. Mathen, M. Racik, J. Madhavan, M.V. Antony-Raj, Investigation of structural, optical and electrical properties of transition metal oxide semiconductor CdO-ZnO nanocomposite and its effective role in the removal of water contaminants. *J. Phys. Chem. Solids* **126**, 322–334 (2018). <https://doi.org/10.1016/j.jpcs.2018.11.012>
18. B.O. Godfrey, W.B. Henry, Structural and optical characterization of CdO-ZnO nanocomposite deposited by sol-gel method. *Int. Res. J. Multidiscip. Sci. Technol.* **2**(3), 15–19 (2018)
19. Z.N. Abdul-Ameer, I.R. Agool, Structural and optical properties of ZnO-CdO nanocomposite using electrodeposition method. *Int. Lett. Chem. Phys. Astronomy* **63**, 127–133 (2016)
20. C. Karunakaran, A. Vijayabalan, P. Vinayagamoorthy, CdO-implanted hexagonal ZnO nanoplatelets: red-shifted emission and enhanced charge carrier-resistance and bacteria-inactivation. *Appl. Phys. A* **125**, 14 (2019). <https://doi.org/10.1007/s00339-018-2318-6>
21. P. Senthil Kumar, M. Selvakumar, P. Bhagabati, B. Bharathi, S. Karuthapandian, S. Balakumar, CdO/ZnO nanohybrids: Facile synthesis and morphologically enhanced photocatalytic performance. *RSC Adv.* **4**, 32977–32986 (2014). <https://doi.org/10.1039/C4RA02502D>
22. S.P. Meshram, J.D. Ambekar, I.S. Mulla, D.P. Amalnerkar, P.V. Adhyapak, Synthesis and characterization of CdO-ZnO nanocomposite for degradation of reactive red 198 under ultrasound irradiation. *J. Nanoeng. Nanomanuf.* **4**, 127–134 (2014). <https://doi.org/10.1166/jnan.2014.1181>
23. J.K. Rajput, T.K. Pathak, V. Kumar, H.C. Swart, L.P. Purohit, Liquid petroleum gas sensing application of ZnO/CdO:ZnO nanocomposite at low temperature. *AIP Conf. Proc.* **2018**, 80035 (2014). <https://doi.org/10.1063/1.5028869>
24. R. Saravanan, F. Gracia, M.M. Khan, V. Poornima, V.K. Gupta, V. Narayanan, A. Stephenh, ZnO/CdO nanocomposite for textile effluent degradation and electrochemical detection. *J. Mol. Liq.* **209**, 374–380 (2015). <https://doi.org/10.1016/j.molliq.2015.05.040>
25. G. Somasundaram, J. Rajana, J. Poul, Effect of calcination process on CdO-ZnO nanocomposite by honey-assisted combustion method for antimicrobial performances. *Toxicol. Res.* **7**, 779–789 (2018). <https://doi.org/10.1039/C8TX00059J>
26. S.S. Khan, Enhancement of visible light photocatalytic activity of CdO modified ZnO nanohybrid particles. *J. Photochem. Photobiol. B* **142**, 1–7 (2014). <https://doi.org/10.1016/j.jphotobiol.2014.11.001>
27. A. Umar, M.S. Akhtar, M.S. Al-Assiri, A.E. Al-Salami, S.H. Kim, Composite CdO-ZnO hexagonal nanocones: efficient materials for photovoltaic and sensing applications. *Ceram. Int.* **44**, 5 (2017). <https://doi.org/10.1016/j.ceramint.2017.12.098>
28. R.A. Zargar, A.H. Shah, M. Arora, F.A. Mir, Crystallographic, spectroscopic and electrical study of ZnO:CdO nanocomposite-coated films for photovoltaic applications. *Arab. J. Sci. Eng.* **44**, 6631–6636 (2019). <https://doi.org/10.1007/s13369-019-03823-9>

29. T. Sinha, M. Ahmaruzzaman, High-value utilization of egg shell to synthesize Silver and Gold-Silver core shell nanoparticles and their application for the degradation of hazardous dyes from aqueous phase-A green approach. *J. Colloid Interface Sci.* **453**, 115–131 (2015). <https://doi.org/10.1016/j.jcis.2015.04.053>
30. J. Celina Selvakumari, S.T. Nishanthi, J. Dhanalakshmi, M. Ahila, D. Pathinettam Padiyan, Bio-active synthesis of tin oxide nanoparticles using eggshell membrane for energy storage application. *Appl. Surf. Sci.* **441**, 530–537 (2018). <https://doi.org/10.1016/j.apsusc.2018.02.043>
31. S. Albohani, M.M. Sundaram, D.W. Laird, Egg shell membrane template stabilises formation of β -NiMoO₄ nanowires and enhances hybrid supercapacitor behaviour. *Mater. Lett.* **236**, 64–68 (2019). <https://doi.org/10.1016/j.matlet.2018.10.034>
32. P.S. Devi, S. Banerjee, S.R. Chowdhury, G.S. Kumar, Eggshell membrane: a natural biotemplate to synthesize fluorescent gold nanoparticles. *RSC Adv.* **2**, 11578–11585 (2012). <https://doi.org/10.1039/C2RA21053C>
33. B. Zheng, L. Qian, H. Yuan, D. Xiaoa, X. Yangc, M.C. Paaud, M.M.F. Choid, Preparation of gold nanoparticles on eggshell membrane and their biosensing application. *Talanta* **82**(1), 177–183 (2010). <https://doi.org/10.1016/j.talanta.2010.04.014>
34. Q. Dong, Su Huilan, Di Zhang, Na Zhu, X. Guo, Biotemplate-directed assembly of porous SnO₂ nanoparticles into tubular hierarchical structures. *Scr. Mater.* **55**(9), 799–802 (2006). <https://doi.org/10.1016/j.scriptamat.2006.07.012>
35. S. Fan, M. Zhao, L. Ding, J. Liang, J. Chen, Y. Li, S. Chen, Synthesis of 3Dhierarchical porous Co₃O₄ film by egg shell membrane for non-enzymatic glucose detection. *J. Electroanal. Chem.* **775**, 52–57 (2016). <https://doi.org/10.1016/j.jelechem.2016.05.035>
36. J. Li, D. Zhai, F. Lv, Yu Qingqing, H. Ma, J. Yin, Z. Yi, M. Liu, J. Chang, Wu Chengtie, Preparation of copper-containing bioactive glass/eggshell membrane nanocomposite for improving angiogenesis, antibacterial activity and wound healing. *Acta Biomater.* **36**, 254–266 (2016). <https://doi.org/10.1016/j.actbio.2016.03.011>
37. M. Liang, Su Rongxin, W. Qi, Yu Yanjun, L. Wang, Z. He, Synthesis of well-dispersed Ag nanoparticles on eggshell membrane for catalytic reduction of 4-nitrophenol. *J. Mater. Sci.* **49**, 1639–1647 (2014). <https://doi.org/10.1007/s10853-013-7847-y>
38. M. Prekajski, B. Babic, D. Bucevac, J. Pantić, J. Gulicovski, M. Miljkovic, B. Matović, Synthesis and characterization of biomorphic CeO₂ obtained by using egg shell membrane as template. *Process. Appl. Ceram.* **8**(2), 81–85 (2014). <https://doi.org/10.2298/PAC1402081P>
39. Qi Wang, C. Ma, J. Tang, C. Zhang, L. Ma, Eggshell membrane-templated MnO₂ nanoparticles: facile synthesis and tetracycline hydrochloride decontamination. *Nanoscale Res. Lett.* **13**, 255 (2018). <https://doi.org/10.1186/s11671-018-2679-y>
40. R. Camaratta, A.N. Correia-Lima, M.D. Reyes, M.A. Hernández-Fenollosa, J. Orozco-Messana, C.P. Bergmann, Microstructural evolution and optical properties of TiO₂ synthesized by eggshell Membrane templating for DSSCs application. *Mater. Res. Bull.* **48**(4), 1569–1574 (2013). <https://doi.org/10.1016/j.materresbu.2012.12.047>
41. Q. Dong, H. Su, J. Xu, D. Zhang, R. Wang, Synthesis of biomorphic ZnO interwoven microfibers using eggshell membrane as the biotemplate. *Mater. Lett.* **61**(13), 2714–2717 (2007). <https://doi.org/10.1016/j.matlet.2006.06.091>
42. N. Song, H. Jiang, T. Cui, L. Chang, X. Wang, Synthesis and enhanced gas-sensing properties of mesoporous hierarchical α -Fe₂O₃ architectures from an eggshell membrane. *Micro Nano Lett.* **7**(9), 943–946 (2012). <https://doi.org/10.1049/mnl.2012.0631>
43. X. He, D.-P. Yanga, X. Zhang, M. Liu, Z. Kang, C. Lin, N. Jia, R. Luque, Waste eggshell membrane-templated CuO-ZnO nanocomposite with enhanced adsorption, catalysis and antibacterial properties for water purification. *Chem. Eng. J.* **369**, 621–633 (2019). <https://doi.org/10.1016/j.cej.2019.03.047>
44. C. Vlgas, S. Machado-de-Souza, E.F.A. Smania, A. Smania Jr., Screening methods to determine antibacterial activity of natural products. *Braz. J. Microbiol.* **38**, 369–380 (2007). <https://doi.org/10.1590/S1517-83822007000200034>
45. S.D. Sarker, L. Nahar, Y. Kumarasamy, Microtitre plate-based antibacterial assay incorporating resazurin as an indicator of cell growth, and its application in the *in vitro* antibacterial screening of phytochemicals. *Methods* **42**, 321–324 (2007). <https://doi.org/10.1016/j.ymeth.2007.01.006>
46. N. Thovhogi, E. Park, E. Manikandan, M. Maaza, A. Gurib-Fakim, Physical properties of CdO nanoparticles synthesized by green chemistry via Hibiscus Sabdariffa flower extract. *J. Alloys Compd.* **655**, 314–320 (2016). <https://doi.org/10.1016/j.jallcom.2015.09.063>
47. P. Senthil Kumar, M. Selvakumar, S. Ganesh-Babu, S. Karuthapandian, S. Chattopadhyay, P. Senthil Kumar, M. Selvakumar, S. Ganesh Babu, S. Karuthapandian, S. Chattopadhyay, CdO nanospheres: Facile synthesis and bandgap modification for the superior photocatalytic activity. *Mater. Lett.* **151**, 45–48 (2015). <https://doi.org/10.1016/j.matlet.2015.03.047>
48. N.C.S. Selvam, R.T. Kumar, K. Yogeenth, L. John-Kennedy, G. Sekaran, J. Judith Vijaya, Simple and rapid synthesis of cadmium oxide (CdO) nanospheres by a microwave-assisted combustion method. *Powder Technol.* **211**(2–3), 250–255 (2011). <https://doi.org/10.1016/j.powtec.2011.04.031>
49. N.D. Krupa, R. Vimala, Evaluation of tetraethoxysilane (TEOS) sol-gel coatings, modified with green synthesized zinc oxide nanoparticles for combating microfouling. *Mater. Sci. Eng. C* **61**, 728–735 (2016). <https://doi.org/10.1016/j.msec.2016.01.013>
50. S. Jafarirad, M. Mehrabi, B. Divband, M. Kosari-Nasab, Biofabrication of zinc oxide nanoparticles using fruit extract of Rosa canina and their toxic potential against bacteria: a mechanistic approach. *Mater. Sci. Eng. C* **59**, 296–302 (2016). <https://doi.org/10.1016/j.msec.2015.09.089>
51. N. Supraja, T.N. Prasad, T. Giridhara-Krishna, E. David, Synthesis, characterization, and evaluation of the antimicrobial efficacy of *Boswellia ovalifoliolata* stem bark-extract-mediated zinc oxide nanoparticles. *Appl. Nanosci.* **6**, 581–590 (2016). <https://doi.org/10.1007/s13204-015-0472-0>
52. K. Qi, B. Cheng, Yu Jiaguo, W. Ho, Review on the improvement of the photocatalytic and antibacterial activities of ZnO. *J. Alloys Compd.* **727**, 792–820 (2017). <https://doi.org/10.1016/j.jallcom.2017.08.142>

Publisher's Note Springer Nature remains neutral with regard to jurisdictional claims in published maps and institutional affiliations.